Supplementary Materials for

High selectivity framework polymer membranes chemically tuned towards fast anion conduction

Junkai Fang[1,2#], Guozhen Zhang[3#], Marc-Antoni Goulet[4], Peipei Zuo[1,2], Yu Zhou[3], Hui Li[1,2], Jun Jiang[1], Michael D. Guiver[5], Zhengjin Yang[1,2]* and Tongwen Xu[1,2]*

[1.] Key Laboratory of Precision and Intelligent Chemistry, University of Science and Technology of China, Hefei, Anhui 230026, P. R. China

[2.] Department of Applied Chemistry, School of Chemistry and Materials Science, University of Science and Technology of China, Hefei, Anhui 230026, P. R. China

[3.] Hefei National Research Center for Physical Sciences at the Microscale, University of Science and Technology of China, Hefei, Anhui 230026, P. R. China

[4.] Department of Chemical and Materials Engineering, Concordia University, Montreal, QC, H3G 1M8, CANADA

[5.] State Key Laboratory of Engines, School of Mechanical Engineering, Tianjin University, Tianjin 300072, P. R. China

# These authors contribute equally.

E-mail: yangzj09@ustc.edu.cn, twxu@ustc.edu.cn

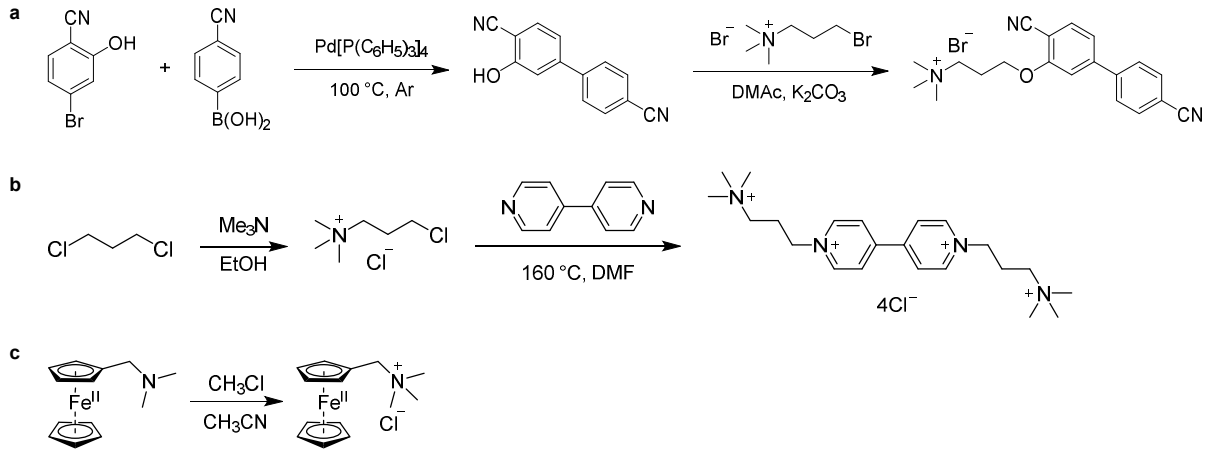

Fig. S1. Synthetic route for **a**) quaternized dicyano monomer (3-((4,4'-dicyano-[1,1'-biphenyl]-3-yl)oxy)-*N,N,N*-trimethylpropan-1-aminium bromide), **b**) bis(3-trimethylammonio)propyl viologen tetrachloride (BTMAP-Vi), and **c**) (ferrocenylmethyl)trimethylammonium chloride (FcNCl).

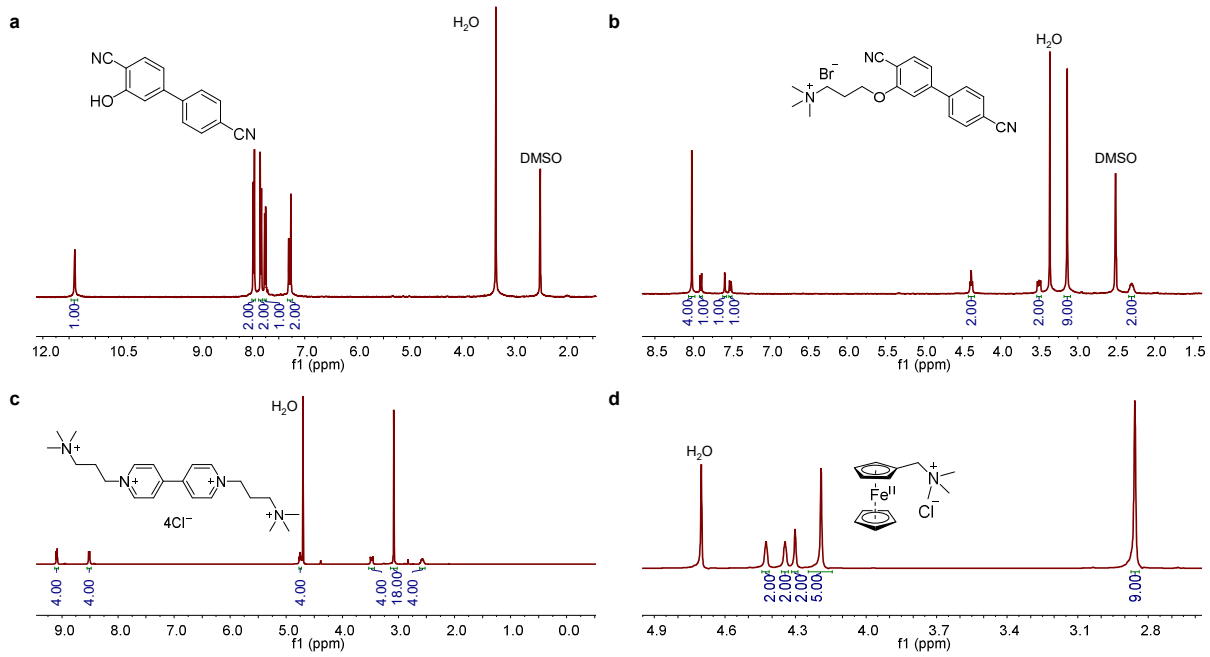

Fig. S2. ^{1}H-NMR spectra of aromatic nitrile monomers (**a, b**) and redox-active organic electrolytes (**c, d**).

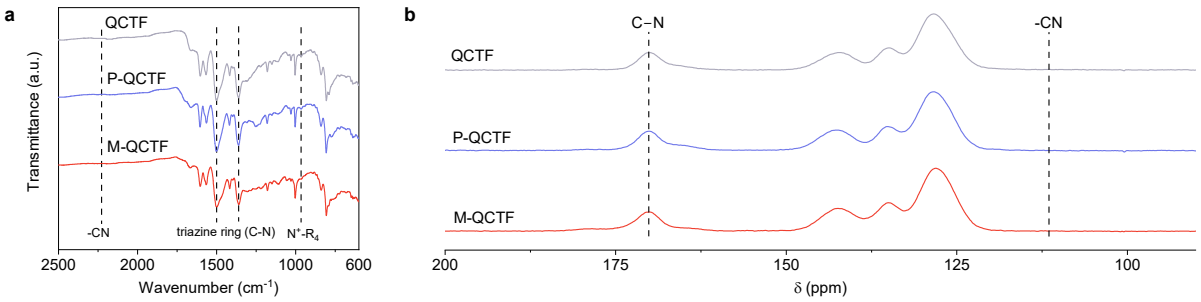

Fig. S3. FTIR spectra (**a**) and solid-state ^{13}C-NMR spectra (**b**) of positively charged covalent triazine framework membranes.

Notes: The characteristic signals of quaternary ammonium groups and triazine rings (C–N) are highlighted with dotted lines. Characteristic peaks of –CN moieties were not found in the FTIR or the ^{13}C-NMR spectra, implying nearly complete conversion of nitrile groups during the modified organic sol–gel process.

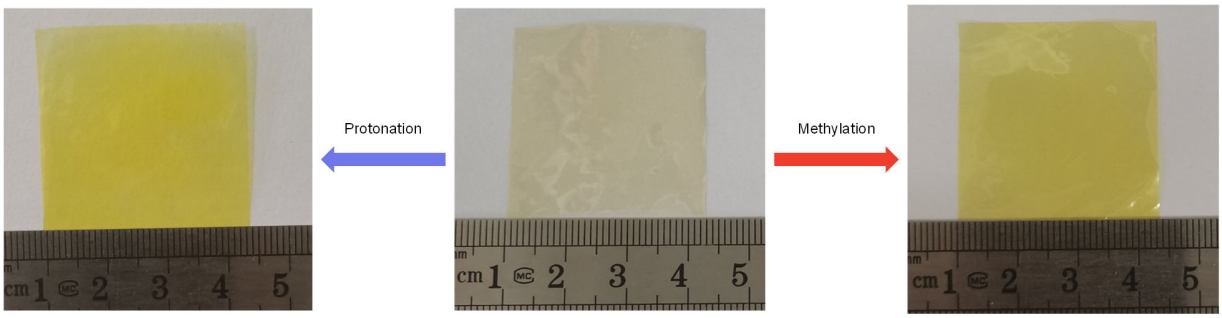

Fig. S4. Photographs of positively charged covalent triazine framework (QCTF) membranes: protonated QCTF (P-QCTF, left), QCTF (middle), and methylated QCTF (M-QCTF, right).

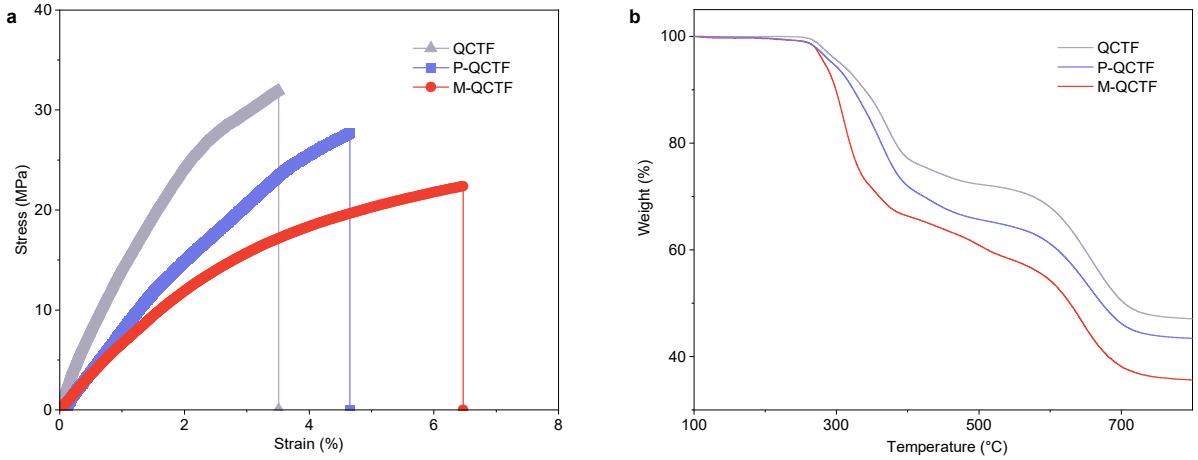

Fig. S5. (**a**) The stress-strain curve measured for QCTF, P-QCTF, and M-QCTF membrane samples. (**b**) TGA curves recorded for QCTF, P-QCTF, and M-QCTF membrane samples under N_2 at a heating rate of 10 ^oC min^{-1}.

Notes: The tensile strengths of QCTF, P-QCTF, and M-QCTF reached 32.0 MPa, 27.7 MPa, and 22.4 MPa, respectively, and their elongations at break were 3.5%, 4.7%, and 6.5%, respectively. The Young's modulus of these membrane samples was calculated to be 0.91 GPa, 0.59 GPa, and 0.34 GPa, respectively. The high Young's modulus and small elongation at break imply the exceptional rigidity of QCTF membrane framework compared with other anion exchange membranes. These membrane samples were thermally stable up to >200 °C.

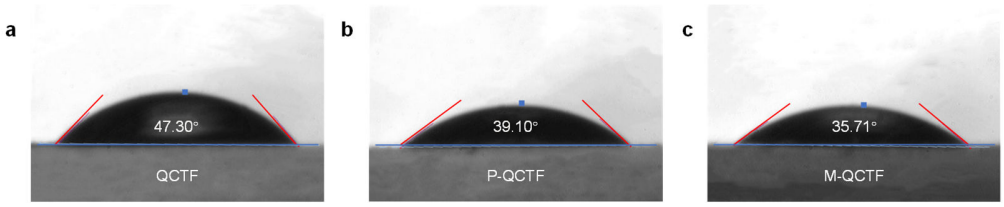

Fig. S6. Static water contact angles of QCTF (**a**), P-QCTF (**b**), and M-QCTF (**c**).

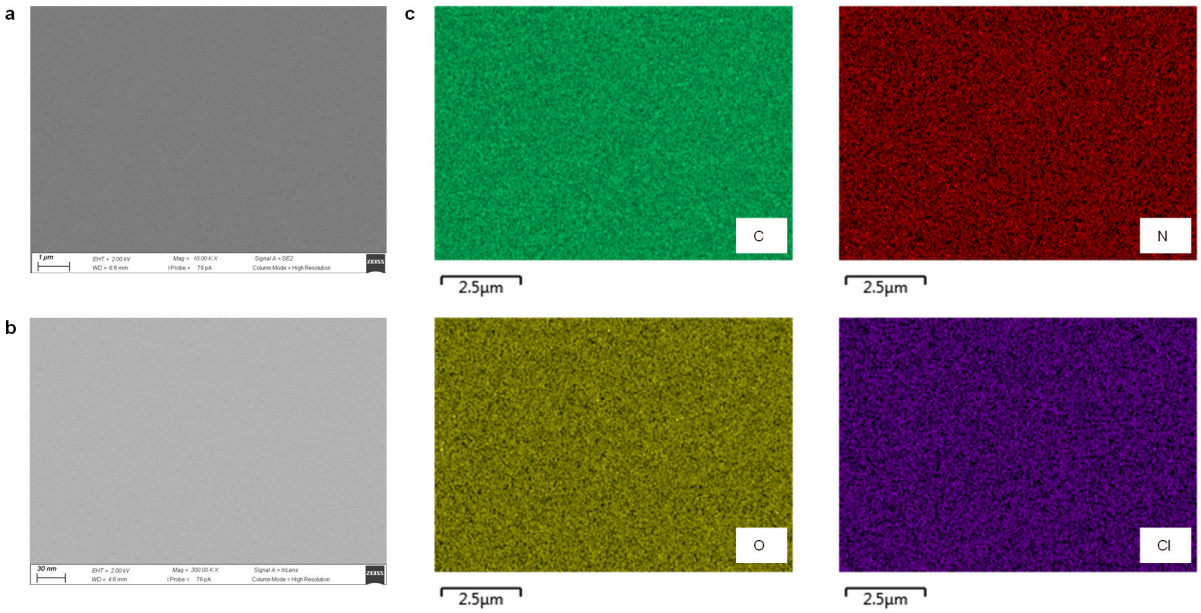

Fig. S7. Surface morphology (**a, b**) and EDS elemental mapping (**c**) for M-QCTF membrane samples.

Notes: The surface SEM images of the M-QCTF membrane sample revealed a uniform and flat morphology, free of defects. The EDS mapping images further demonstrate uniform elemental distributions.

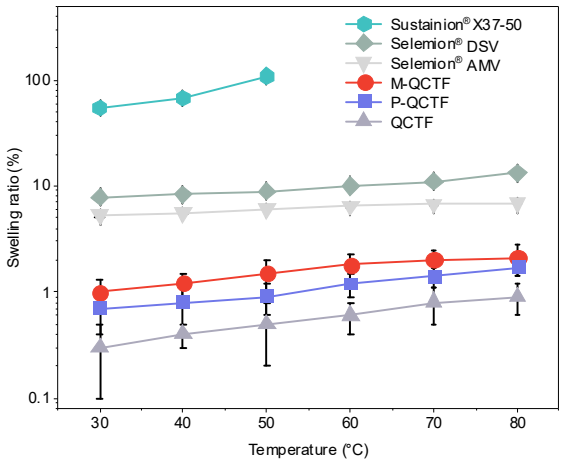

Fig. S8. Swelling ratio of the Sustainion® X37-50, Selemion® DSV, Selemion® AMV, M-QCTF, P-QCTF, and QCTF membranes at various temperatures.

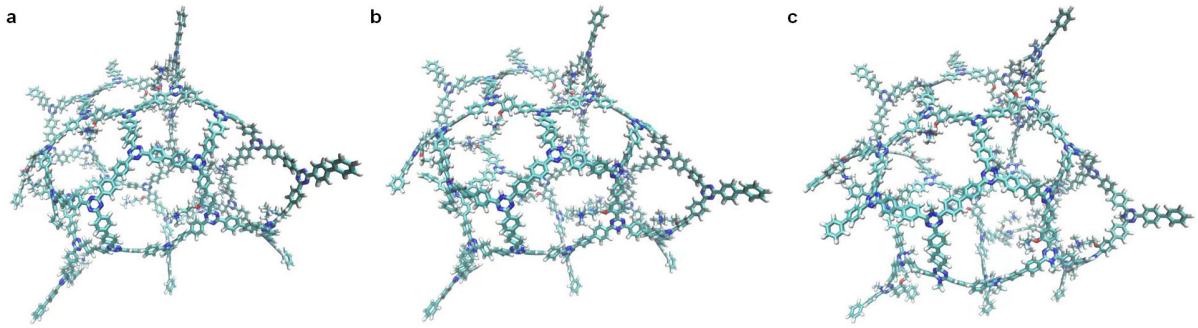

Fig. S9. Stick-filling models of polymer chains for QCTF (**a**), P-QCTF (**b**), and M-QCTF (**c**). A total of 63 repeating units were used to generate these chains. Color code: carbon in cyan, nitrogen in blue, oxygen in red, hydrogen in white.

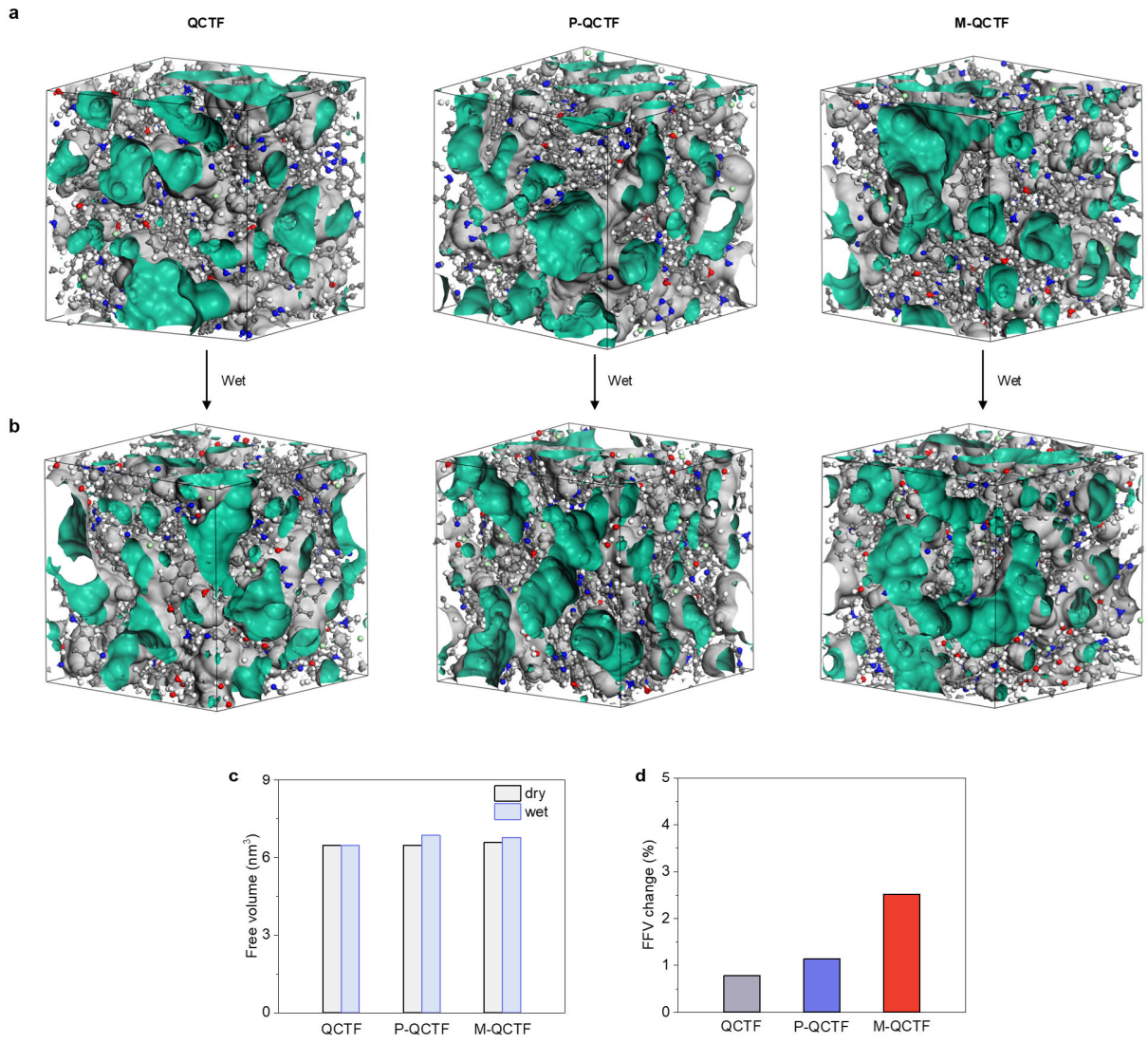

Fig. S10. Porosity analysis for QCTF polymers. Three-dimensional view of the amorphous cells of QCTF, P-QCTF and M-QCTF in the dry (**a**) and wet (**b**) state. Cell size: 29.87 × 29.87 × 29.87 Å^3 for QCTF in the dry state (left in the first row), 30.18 × 30.18 × 30.18 Å^3 for P-QCTF in the dry state (middle in the first row), 30.30 × 30.30 × 30.30 Å^3 for M-QCTF in the dry state (right in the first row), 30.54 × 30.54 × 30.54 Å^3 for QCTF in the wet state (left in the second row), 30.94 × 30.94 × 30.94 Å^3 for P-QCTF in the wet state (middle in the second row), 31.14 × 31.14 × 31.14 Å^3 for M-QCTF in the wet state (right in the second row), respectively. The grey surface indicates the van der Waals surface, and the green surface is the Connolly surface with a probe radius of 1.55 Å. (**c**) The computed free volume of QCTF, P-QCTF and M-QCTF in the dry and wet state. (**d**) The fractional free volume change between polymer samples in the dry state and wet state. The free volume and fractional free volume were derived from (**a**, **b**).

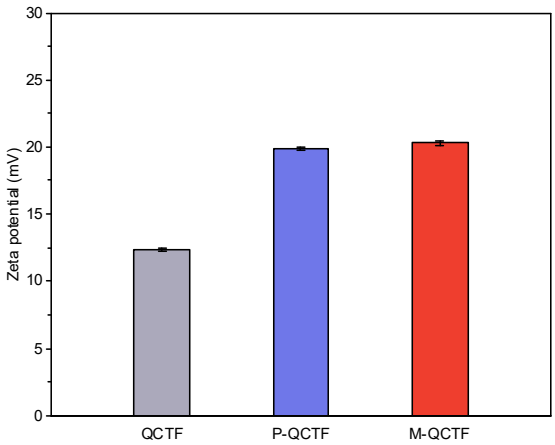

Fig. S11. Zeta potential of positively charged covalent triazine framework (QCTF) membranes.

Notes: The zeta potential was determined to investigate the surface charge of these membranes. To note, the zeta potentials of P-QCTF and M-QCTF were similar, indicating that P-QCTF and M-QCTF had nearly the same degree of protonation or methylation. The ion exchange capacity of the QCTF membranes was titrated to be 1.11±0.19 mmol g^{-1} for QCTF, 2.34±0.45 mmol g^{-1} for P-QCTF and 2.21±0.31 mmol g^{-1}.

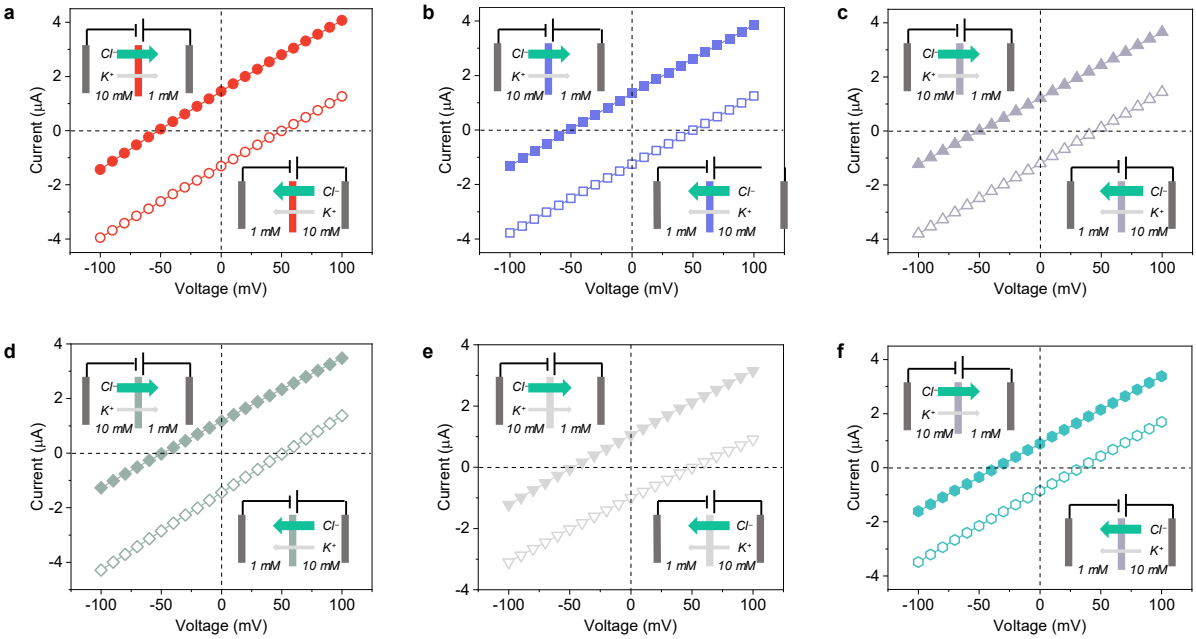

Fig. S12. Current–voltage (I–V) curves recorded for (**a**) M-QCTF, (**b**) P-QCTF, (**c**) QCTF, (**d**) Selemion® DSV, (**e**) Selemion® AMV, and (**f**) Sustainion® X37-50 membranes under a 10-fold KCl concentration gradient across a two-compartment diffusion cell. The curve reflects a net anion flow from the high-concentration compartment to the low-concentration compartment, suggesting anion selectivity. The anion transference number (t_-) of these membranes are derived from the I–V curves. The t_- of M-QCTF, P-QCTF, QCTF, Selemion® DSV, Selemion® AMV, and Sustainion® X37-50 membranes are 0.953, 0.947, 0.94, 0.926, 0.913, and 0.815, respectively.

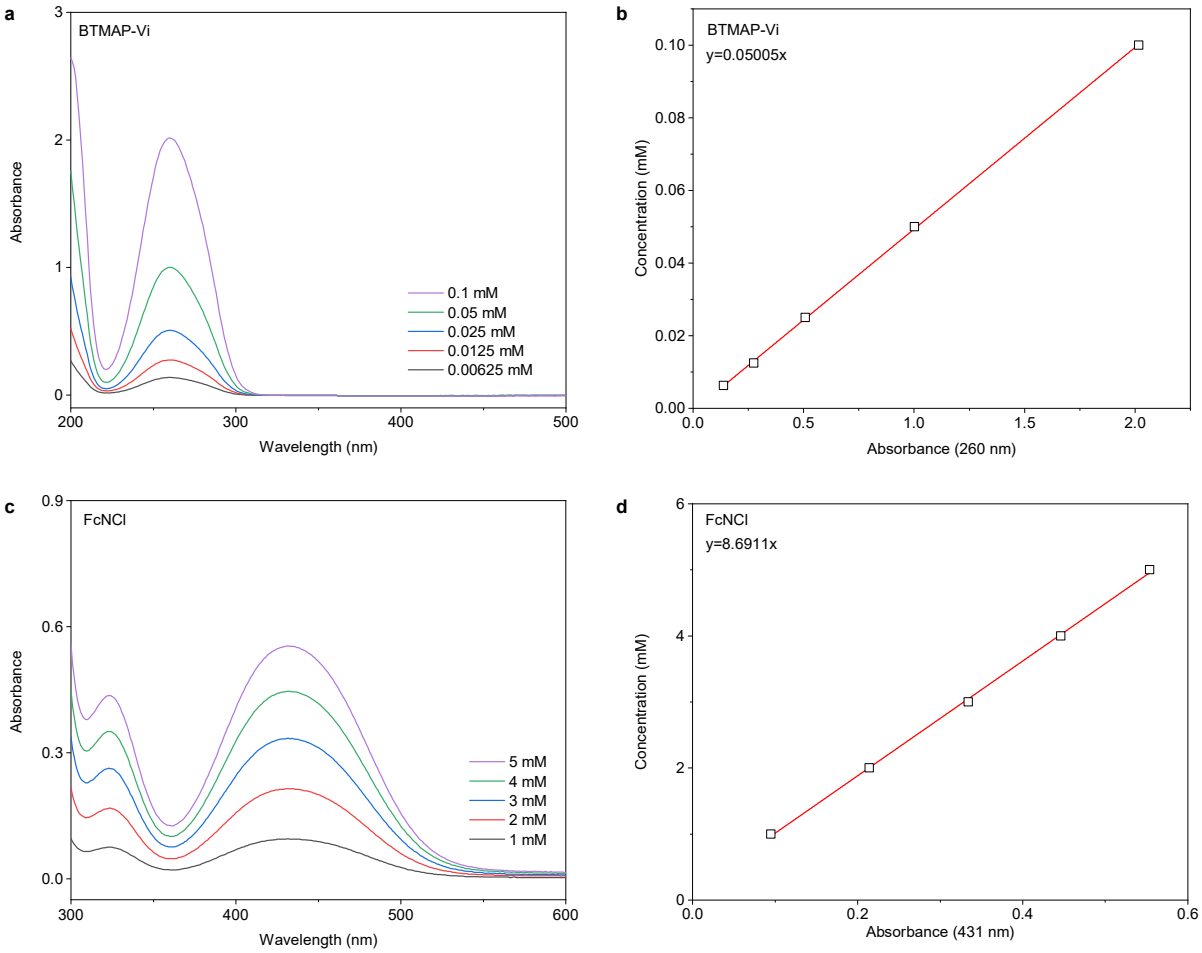

Fig. S13. UV-Vis spectra and the corresponding calibration curves established according to the absorbance at maximum absorption for (**a, b**) BTMAP-Vi and (**c, d**) FcNCl.

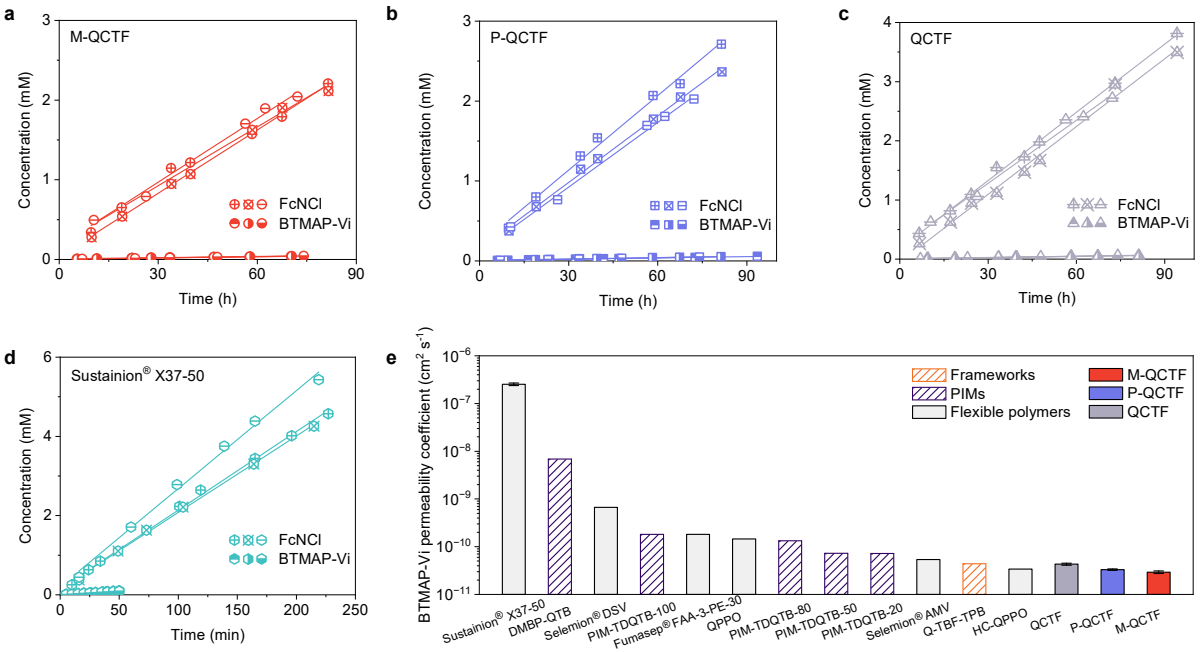

Fig. S14. The concentration of BTMAP-Vi or FcNCl in the receiving compartment of the two-compartment diffusion cell as a function of time, recorded during electrolyte crossover measurements for the M-QCTF (**a**), P-QCTF (**b**), QCTF (**c**) and Sustainion® X37-50 (**d**) membranes. (**e**) Permeability coefficients of BTMAP-Vi across the Selemion® DSV, Selemion® AMV, Sustainion® X37-50, Fumasep® FAA-3-PE-30, QPPO, HC-QPPO, Q-TBF-TPB, PIM-based, QCTFs membranes. To note, 0.01 M BTMAP-Vi was used for the crossover measurement of Sustainion® X37-50 membrane because of fast BTMAP-Vi permeation and detection limit of our apparatus.

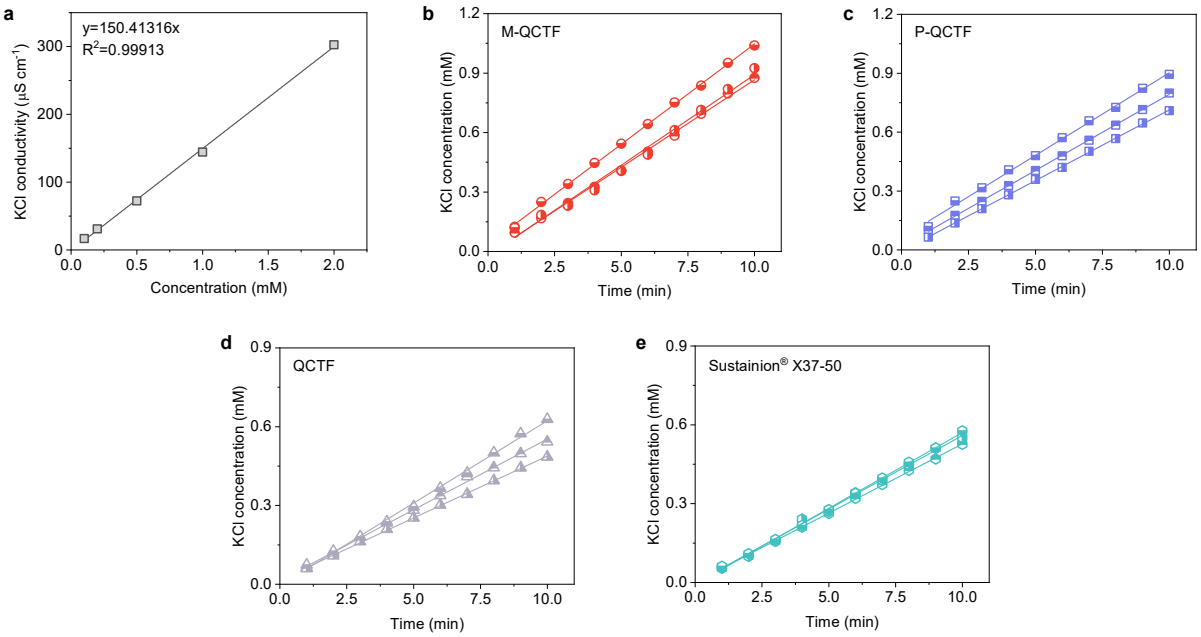

Fig. S15. (**a**) Calibration line of solution conductivity versus the concentration for KCl solution. The concentration of KCl in the receiving compartment of the two-compartment diffusion cell as a function of time, recorded during cross-membrane permeability measurements for the M-QCTF (**b**), P-QCTF (**c**), QCTF (**d**), and Sustainion® X37-50 (**e**) membranes.

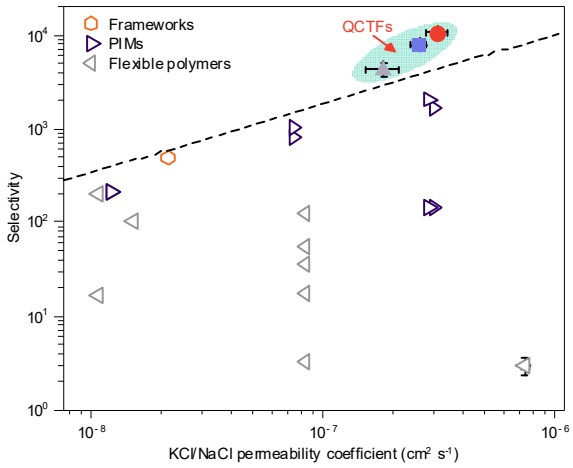

Fig. S16. Comparison of the membrane selectivity and KCl/NaCl permeability coefficient for QCTF membranes, framework membranes, PIM membranes and flexible polymer membranes. The detailed values can be found in Supplementary **Table S6**. The line and the shadow are guides for the eye.

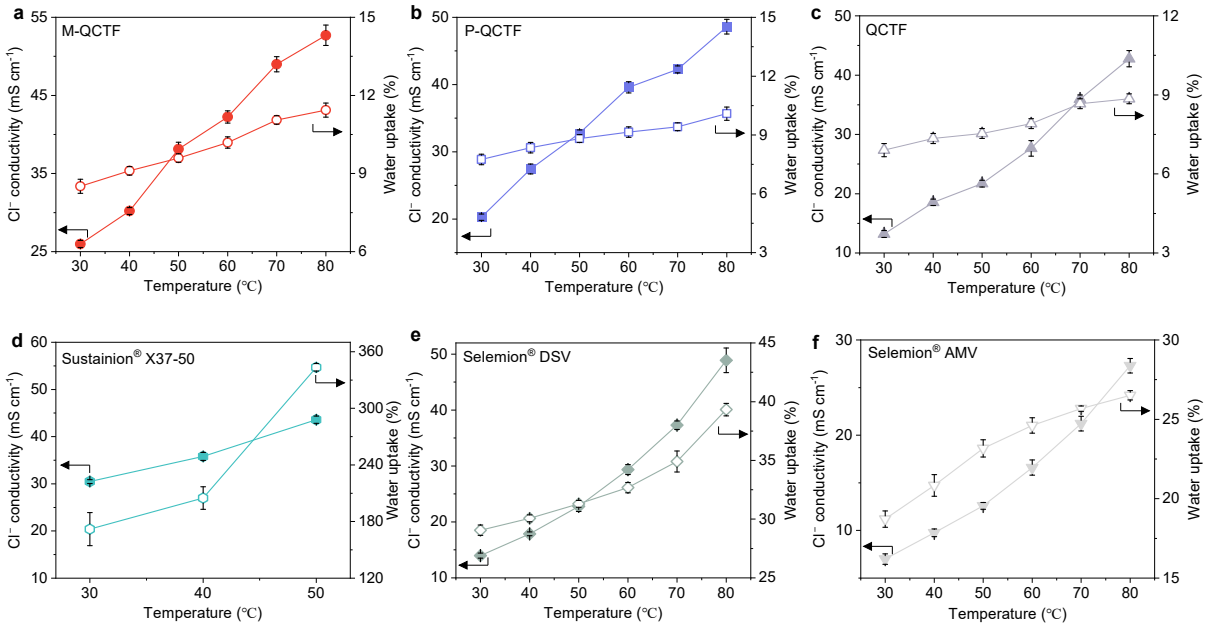

Fig. S17. Cl^- conductivity and membrane water uptake (*WU*) measured at varied temperatures for (**a**) M-QCTF, (**b**) P-QCTF, (**c**) QCTF, (**d**) Sustainion® X37-50, (**e**) Selemion® DSV, and (**f**) Selemion® AMV membranes.

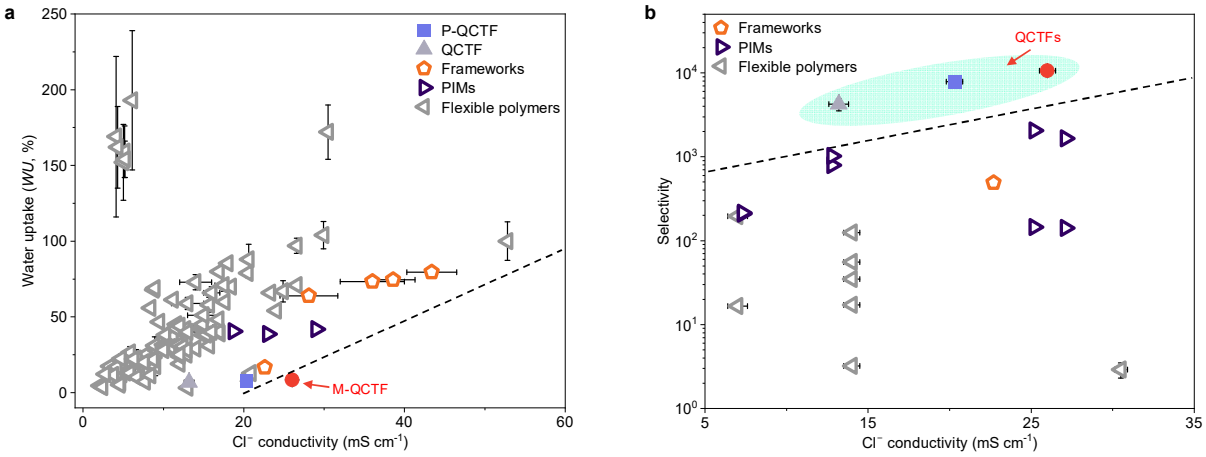

Fig. S18. Upper bound plot for Cl^- conductivity versus water uptake (**a**) and selectivity (**b**) for QCTF membranes, framework membranes, PIM-based membranes, and flexible polymer membranes. The water uptake, and Cl^- conductivity are at 30 °C, 25 °C or room temperature. Selectivity refers to the ratio of the cross-membrane permeability coefficient between the salt ions and bipyridine-based redox-active organic electrolyte. Dashed lines and shades are visual guides. The detailed values can be found in the Supplementary **Table S1** and **S6**.

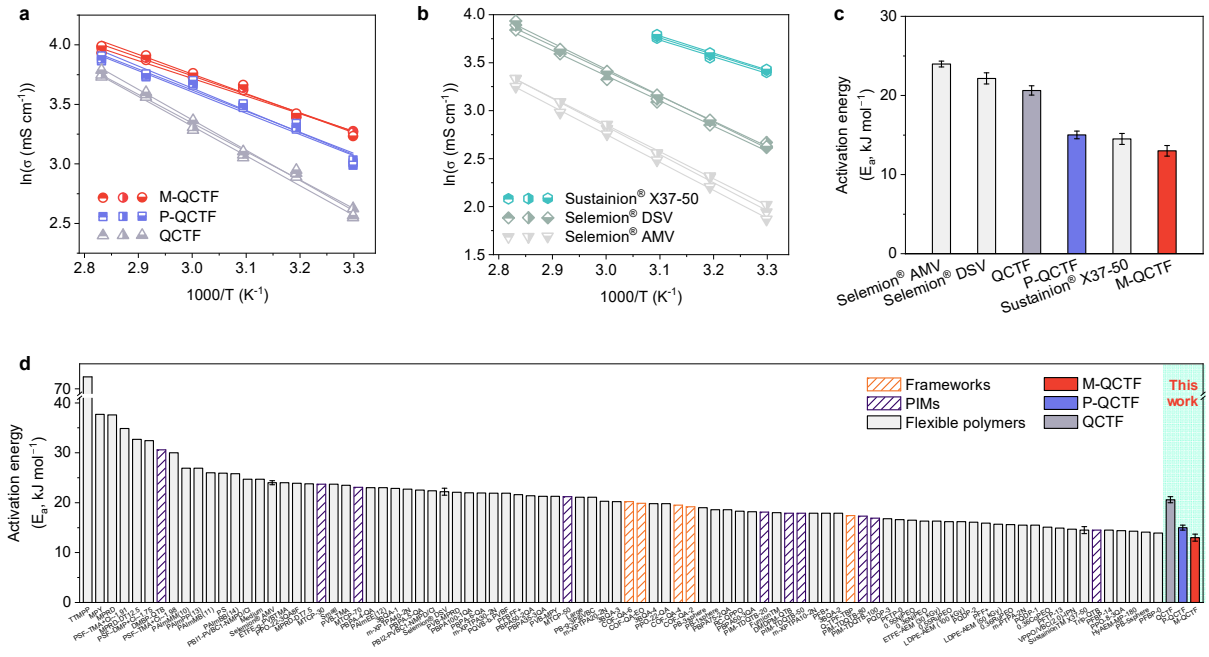

Fig. S19. Temperature dependence of Cl^- conductivities for QCTF membranes (**a**) and commercial AEMs (**b**). (**c**) E_a is derived from the slope of the curve (**a**, **b**) according to the Arrhenius equation. (**d**) Comparison on activation energy for QCTF membranes, framework membranes, PIM-base membranes, and flexible polymer membranes. The detailed values can be found in Supplementary **Table S1**.

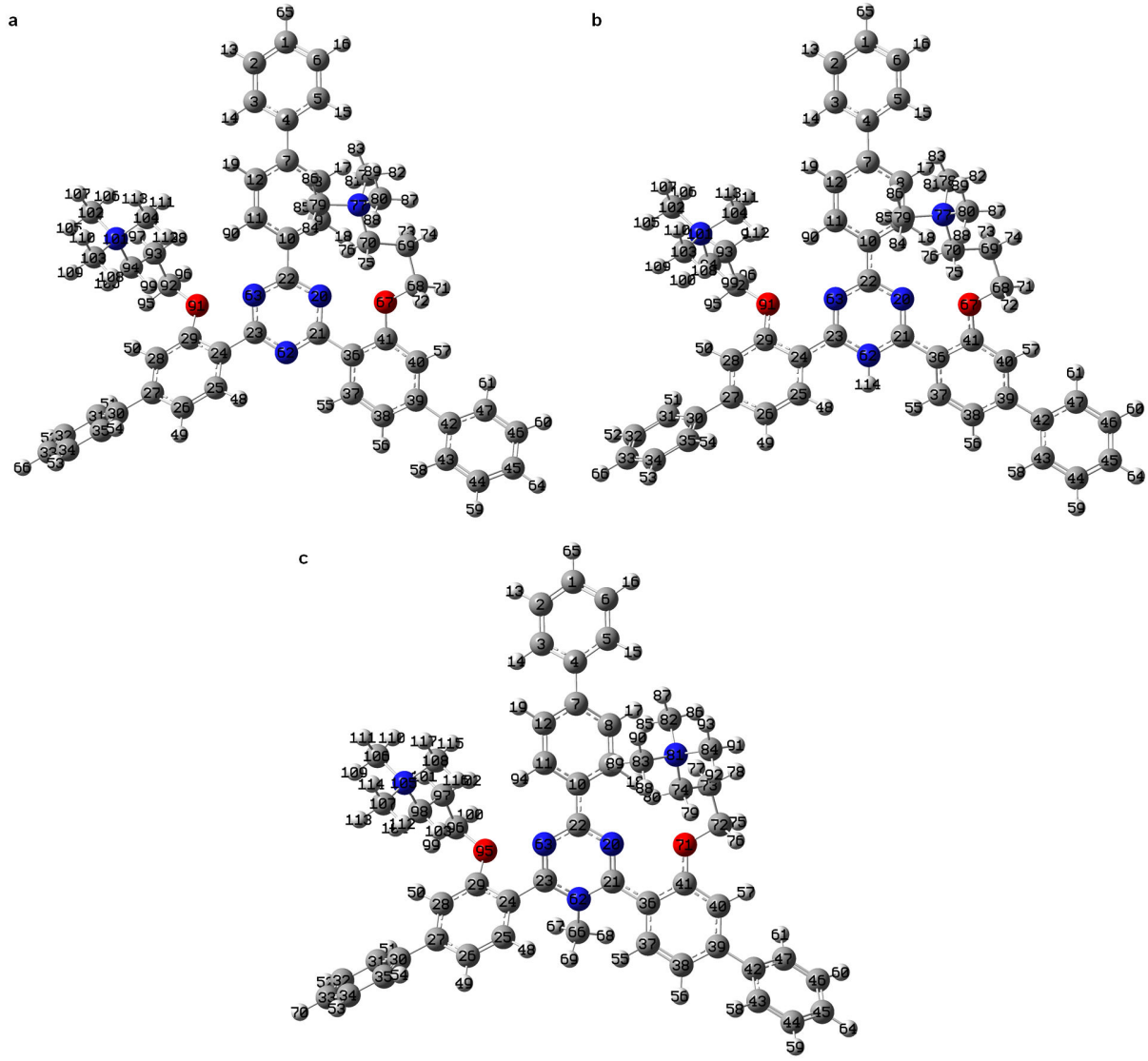

Fig. S20. Atomic numbers of QCTF (**a**), P-QCTF (**b**), and M-QCTF (**c**). Color code: carbon in gray, nitrogen in blue, oxygen in red, hydrogen in white.

Notes: The charge distribution values of different atoms can be found in Supplementary **Table S9**.

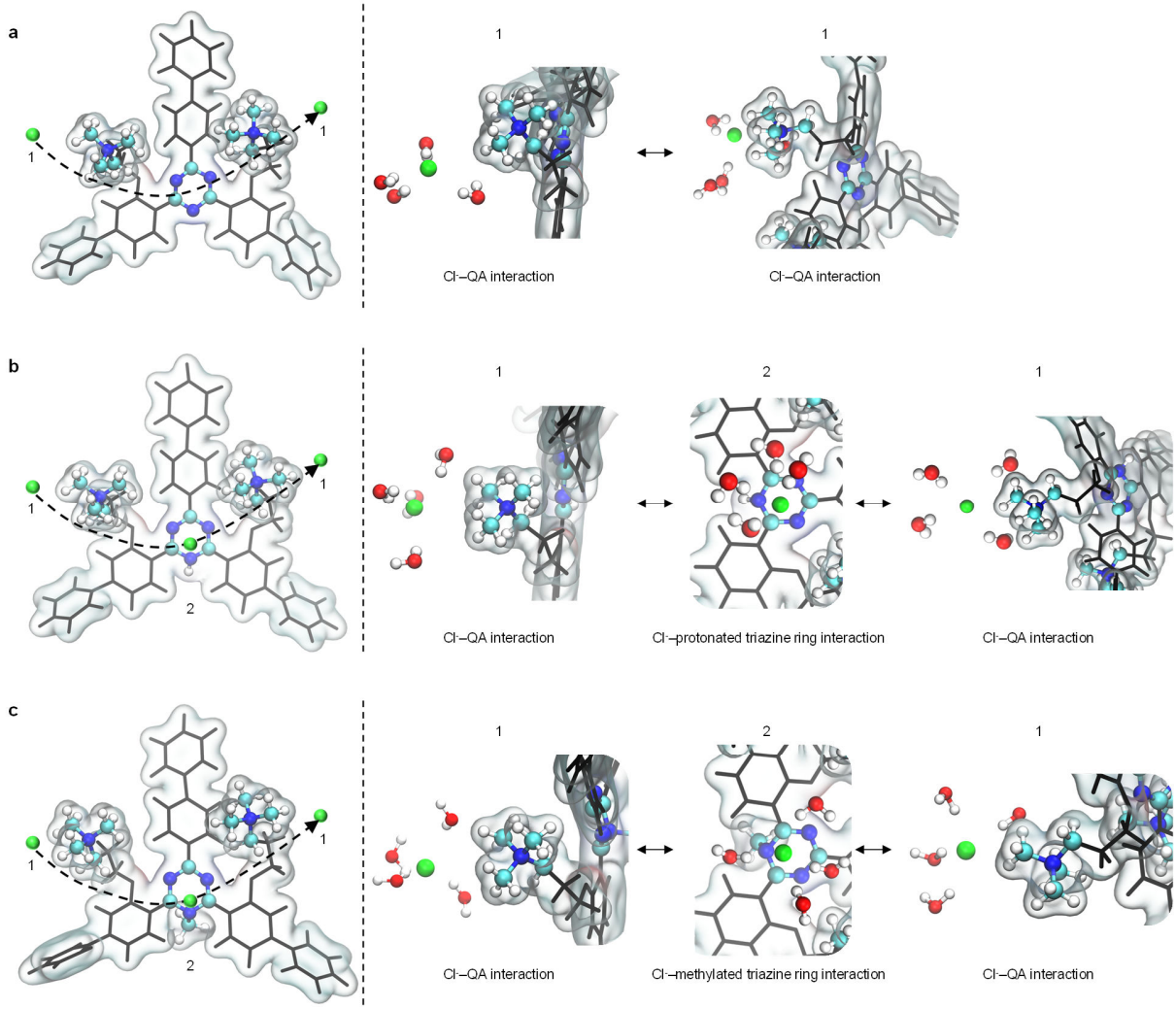

Fig. S21. Snapshots taken during simulation, demonstrating the interactions between Cl^- and the pore walls of QCTF (**a**), P-QCTF (**b**), and M-QCTF (**c**). Insets on the right denote the specific interactions at positions 1 and 2. Color code: carbon in cyan, nitrogen in blue, oxygen in red, hydrogen in white, and chlorine in green.

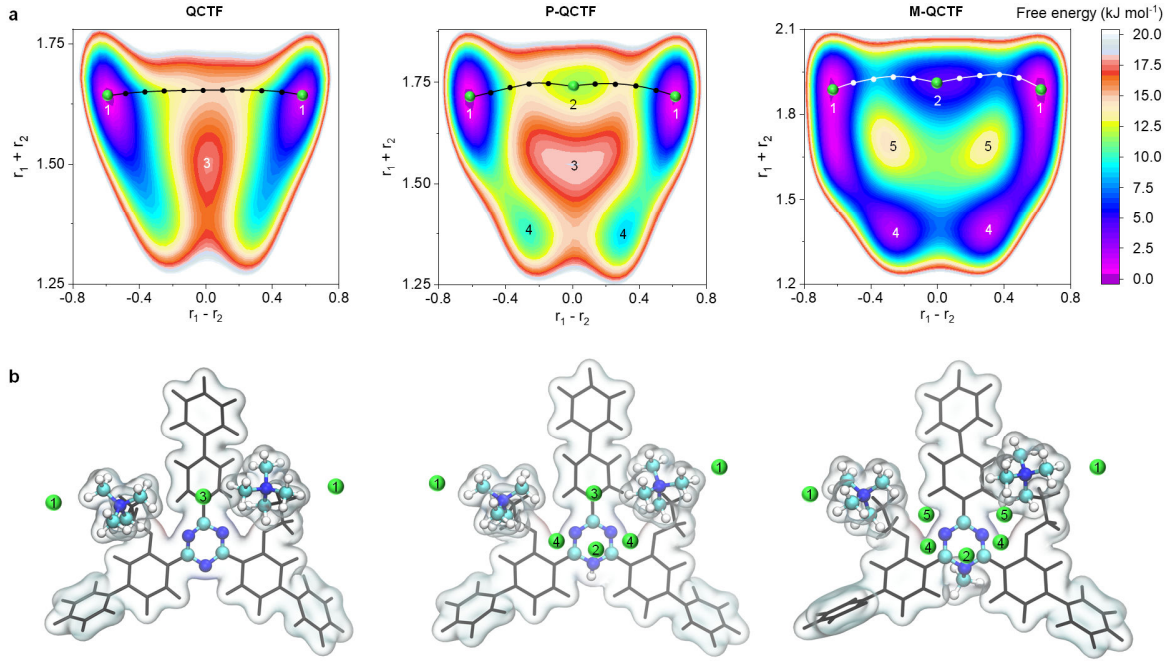

Fig. S22. (**a**) Computed free energy map for the transport of Cl^- ions within the QCTF (left), P-QCTF (middle), and M-QCTF (right) membrane matrices. The black or white lines denote the Cl^- ion transport pathways (1-1 or 1-2-1) with the lowest free energy barrier. (**b**) Snapshots taken during simulation, showing the interactions between Cl^- and the membrane pore walls of QCTF (left), P-QCTF (middle), and M-QCTF (right) at the numbered sites.

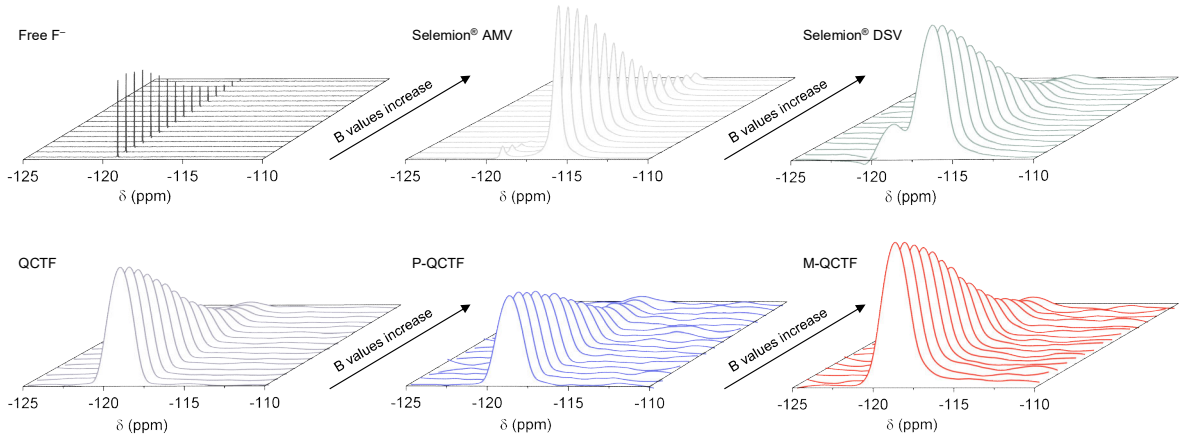

Fig. S23. ^{19}F PFG–NMR spectra recorded for 0.1 M KF solution without membranes (left in the first row) and membrane samples of Selemion® AMV (middle in the first row), Selemion® DSV (right in the first row), QCTF (left in the second row), P-QCTF (middle in the second row) and M-QCTF (right in the second row) immersed in 0.1 M KF solutions, respectively. The membrane samples were placed in NMR tubes during measurements.

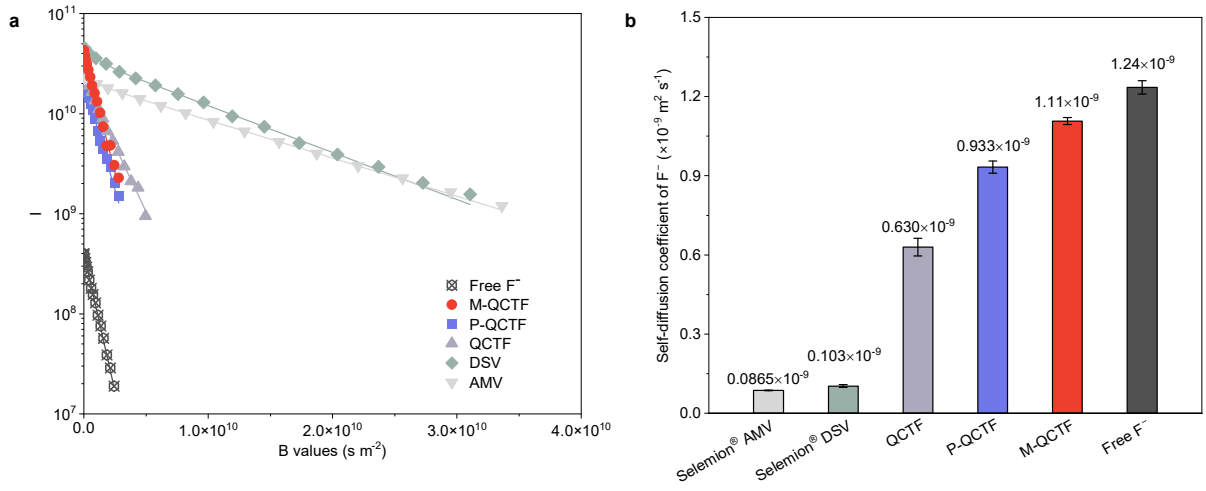

Fig. S24. (**a**) Plot of PFG–NMR signal intensity versus magnetic gradient strength (*B* values) and (**b**) diffusion coefficients derived from PFG–NMR for F^- in water, M-QCTF, P-QCTF, QCTF, Selemion® DSV, and Selemion® AMV membrane samples. Echo profiles are fitted to the Stejskal–Tanner equation. *I* denotes the echo height at a given gradient strength; *B* denotes the product of all parameters before the diffusion coefficient (*D*) of the Stejskal–Tanner equation (that is, equation 13). Error bars (s.d.) are derived from three measurements based on three parallel experiments.

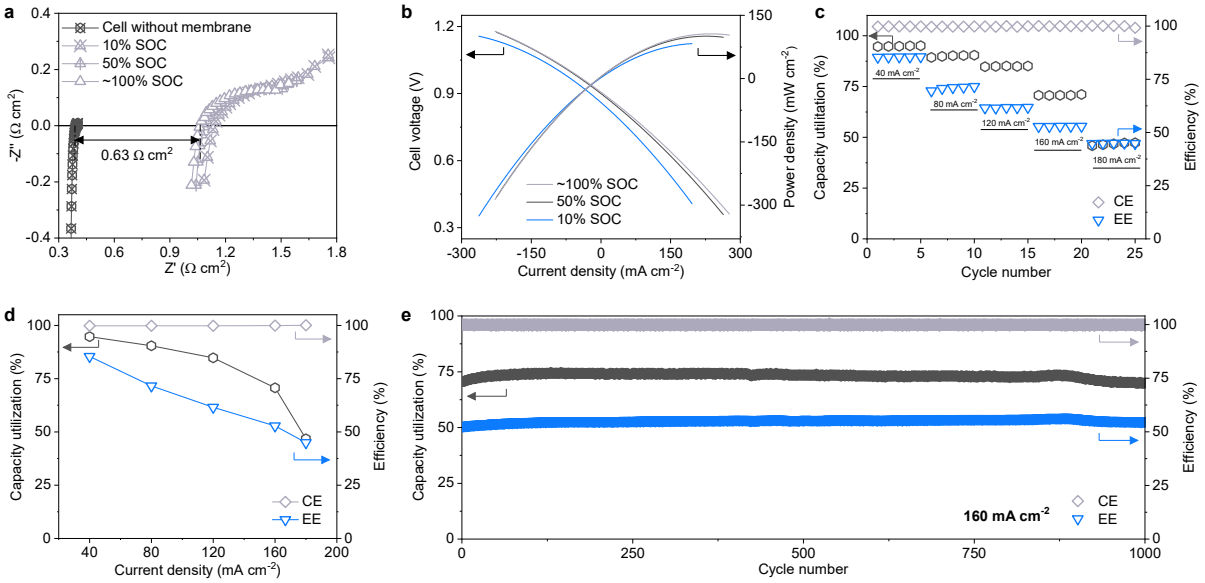

Fig. S25. Performance of a 0.1 M BTMAP-Vi/FcNCl cell assembled with the QCTF membrane. (**a**) EIS spectra and (**b**) polarization curves at various SOCs. (**c, d**) The capacity utilization, Coulombic efficiency (CE), and energy efficiency (EE) at various current densities. (**e**) Long-term galvanostatic cycling of the cell over 1000 cycles (25.2 h) at 160 mA cm^{-2}. The capacity utilization, Coulombic efficiency, and energy efficiency are plotted against the cycle number.

Notes: At 0.1 M, the BTMAP-Vi/FcNCl cell assembled with the QCTF membrane can achieve a low capacity fade rate of 0.0011% per cycle (0.045% per h) over 1000 cycles (25.2 h) at 160 mA cm^{-2}.

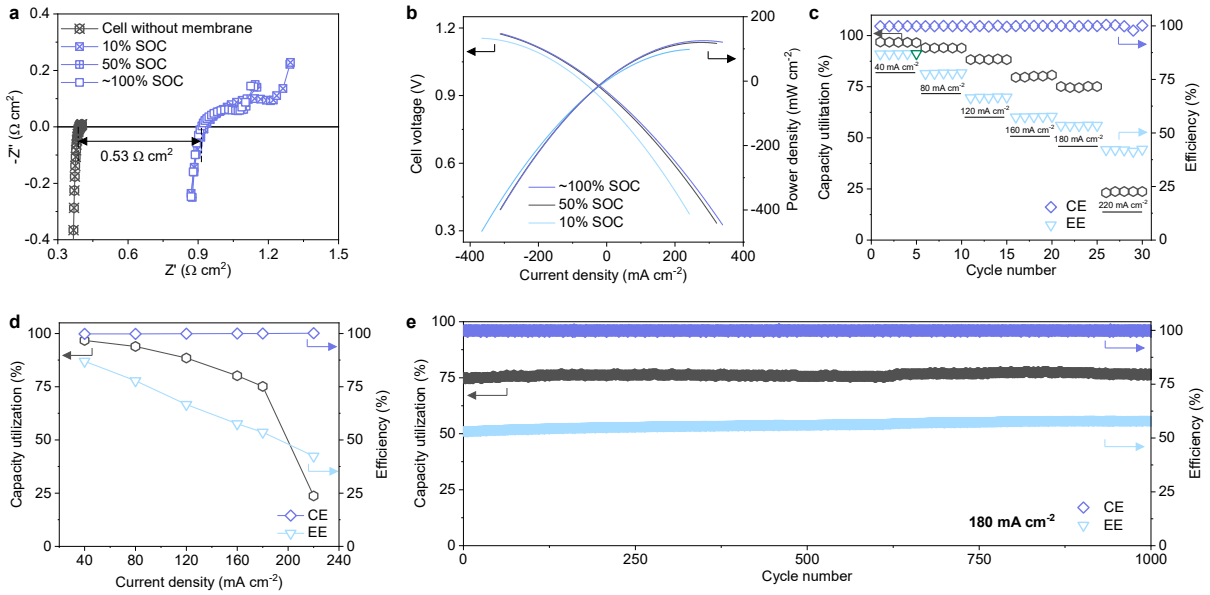

Fig. S26. Performance of a 0.1 M BTMAP-Vi/FcNCl cell assembled with the P-QCTF membrane. (**a**) EIS spectra and (**b**) polarization curves at various SOCs. (**c, d**) The capacity utilization, Coulombic efficiency (CE), and energy efficiency (EE) at various current densities. (**e**) Long-term galvanostatic cycling of the cell over 1000 cycles (21.3 h) at 180 mA cm^{-2}. The capacity utilization, Coulombic efficiency, and energy efficiency are plotted against the cycle number.

Notes: At 0.1 M, the BTMAP-Vi/FcNCl cell assembled with the P-QCTF membrane can effectively retain its capacity for over 1000 cycles (21.3 h) at 180 mA cm^{-2}.

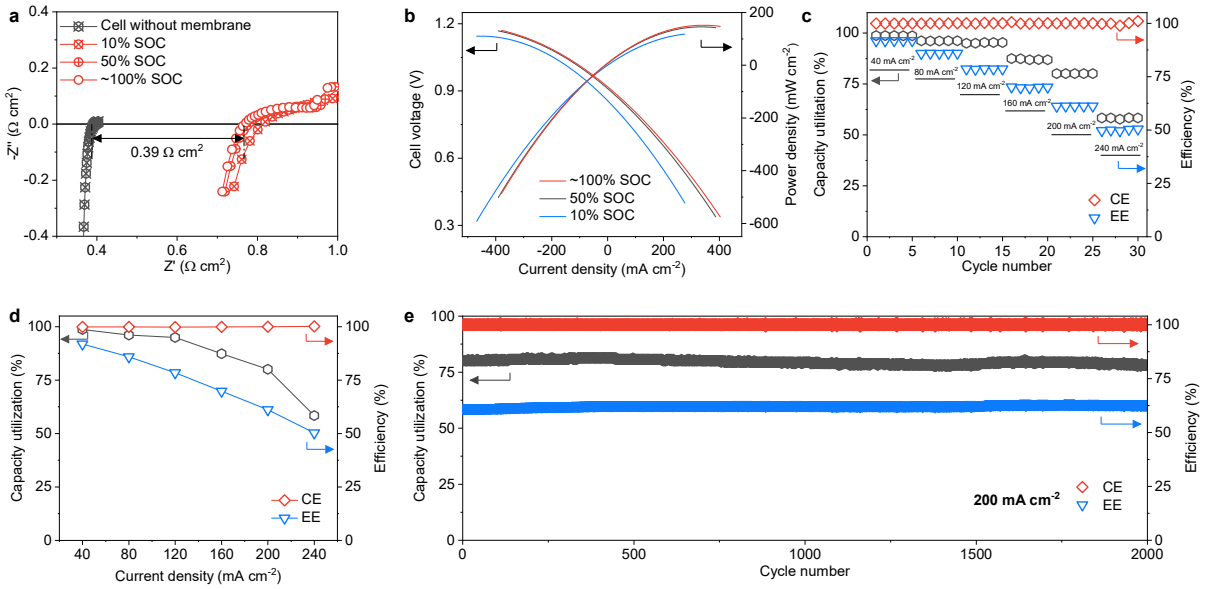

Fig. S27. Performance of a 0.1 M BTMAP-Vi/FcNCl cell assembled with the M-QCTF membrane. (**a**) EIS spectra and (**b**) polarization curves at various SOCs. (**c, d**) The capacity utilization, Coulombic efficiency (CE), and energy efficiency (EE) at various current densities. (**e**) Long-term galvanostatic cycling of the cell over 2000 cycles (41.7 h) at 200 mA cm^{-2}. The capacity utilization, Coulombic efficiency, and energy efficiency are plotted against the cycle number.

Notes: At 0.1 M, the BTMAP-Vi/FcNCl cell assembled with the M-QCTF membrane can achieve a low capacity fade rate of 0.0012% per cycle (0.058% per h) over 2000 cycles (41.7 h) at 200 mA cm^{-2}.

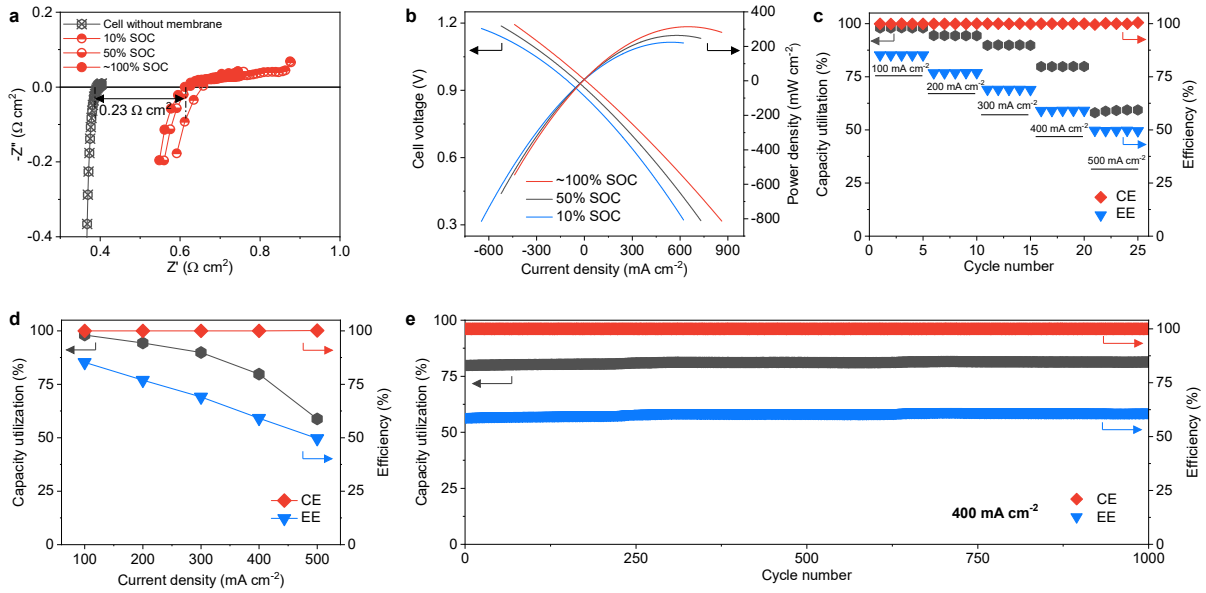

Fig. S28. Performance of a 0.5 M BTMAP-Vi/FcNCl cell assembled with the M-QCTF membrane. (**a**) EIS spectra and (**b**) polarization curves at various SOCs. (**c, d**) The capacity utilization, Coulombic efficiency (CE), and energy efficiency (EE) at various current densities. (**e**) Long-term galvanostatic cycling of the cell over 1000 cycles (54.2 h) at 400 mA cm^{-2}. The capacity utilization, Coulombic efficiency, and energy efficiency are plotted against the cycle number.

Notes: At 0.5 M, the BTMAP-Vi/FcNCl cell assembled with the M-QCTF membrane can effectively retain its capacity for over 1000 cycles (54.2 h) at 400 mA cm^{-2}.

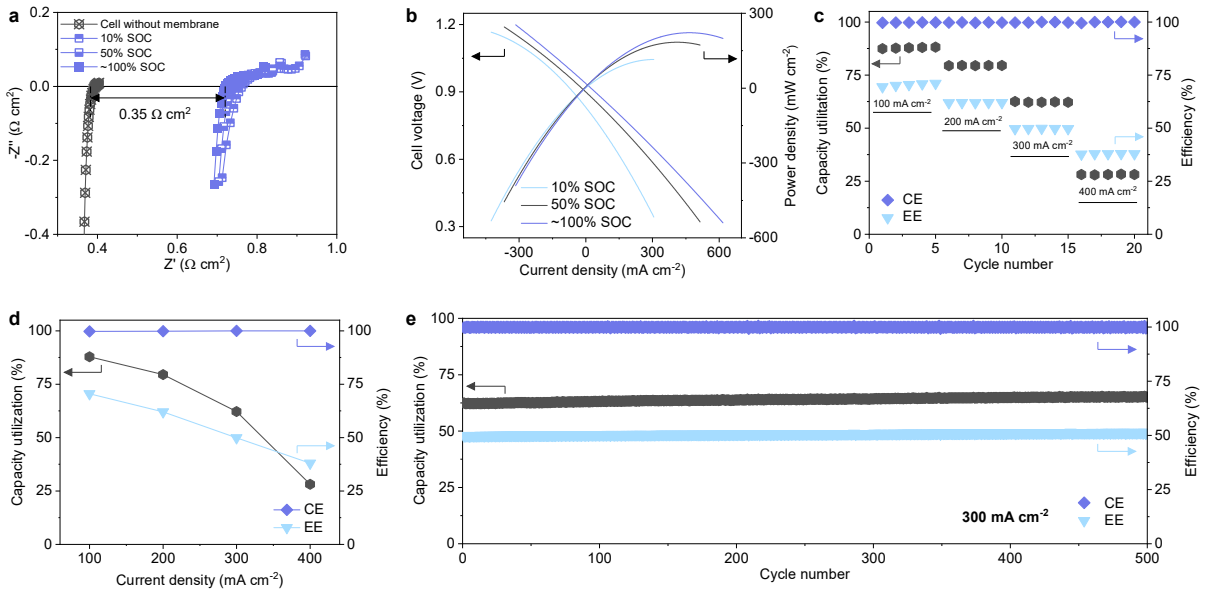

Fig. S29. Performance of a 0.5 M BTMAP-Vi/FcNCl cell assembled with P-QCTF membrane. (**a**) EIS spectra and (**b**) polarization curves at various SOCs. (**c, d**) The capacity utilization, Coulombic efficiency (CE), and energy efficiency (EE) at various current densities. (**e**) Long-term galvanostatic cycling of the cell over 500 cycles (28.5 h) at 300 mA cm^{-2}. The capacity utilization, Coulombic efficiency, and energy efficiency are plotted against the cycle number.

Notes: At 0.5 M, the BTMAP-Vi/FcNCl cell assembled with the P-QCTF membrane can effectively retain its capacity for over 500 cycles (28.5 h) at 300 mA cm^{-2}.

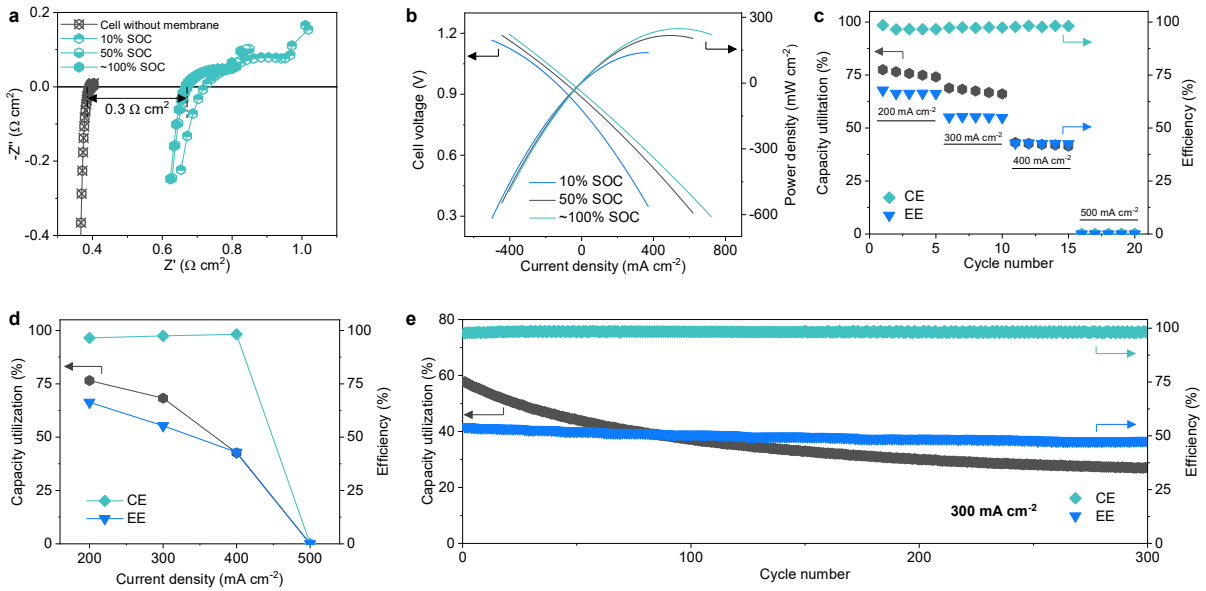

Fig. S30. Performance of a 0.5 M BTMAP-Vi/FcNCl cell assembled with Sustainion® X37-50 membrane. (**a**) EIS spectra and (**b**) polarization curves at various SOCs. (**c, d**) The capacity utilization, Coulombic efficiency (CE), and energy efficiency (EE) at various current densities. (**e**) Long-term galvanostatic cycling of the cell over 300 cycles (8.6 h) at 300 mA cm^{-2}. The capacity utilization, Coulombic efficiency, and energy efficiency are plotted against the cycle number.

Notes: At 0.5 M, the BTMAP-Vi/FcNCl cell assembled with the Sustainion® X37-50 membrane showed a rapid capacity fade rate of 0.24% per cycle (8.4% per h) over 300 cycles (8.6 h) at 300 mA cm^{-2}.

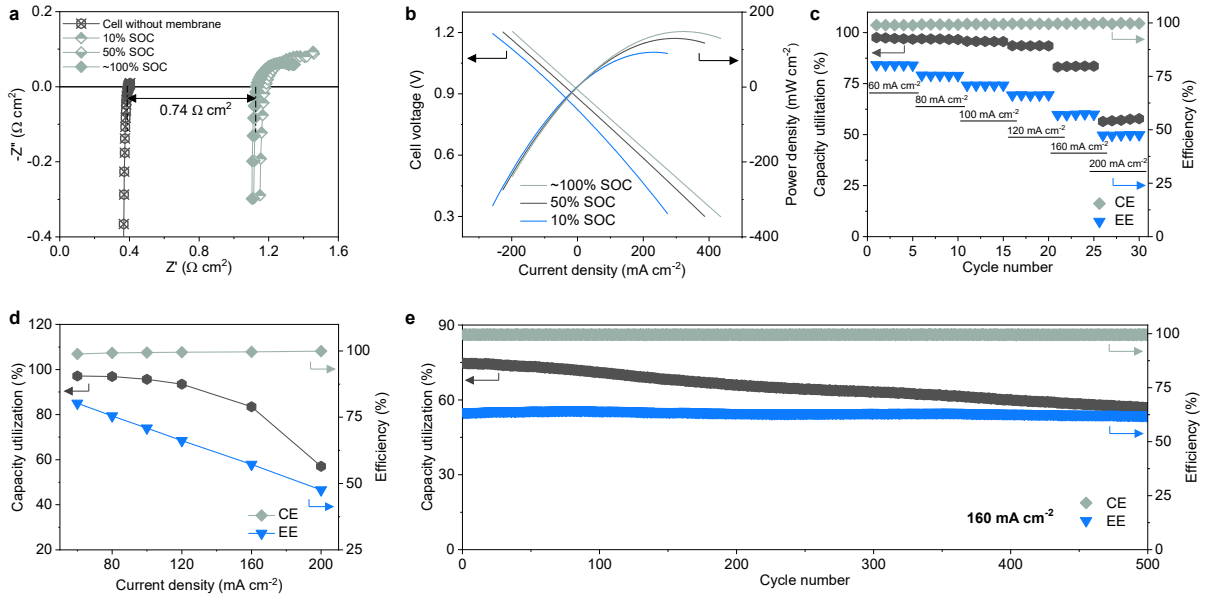

Fig. S31. Performance of a 0.5 M BTMAP-Vi/FcNCl cell assembled with Selemion® DSV membrane. (**a**) EIS spectra and (**b**) polarization curves at various SOCs. (**c, d**) The capacity utilization, Coulombic efficiency (CE), and energy efficiency (EE) at various current densities. (**e**) Long-term galvanostatic cycling of the cell over 500 cycles (44.6 h) at 160 mA cm^{-2}. The capacity utilization, Coulombic efficiency, and energy efficiency are plotted against the cycle number.

Notes: At 0.5 M, the BTMAP-Vi/FcNCl cell assembled with the Selemion® DSV membrane showed a high capacity fade rate of 0.047% per cycle (0.53% per h) over 500 cycles (44.6 h) at 160 mA cm^{-2}.

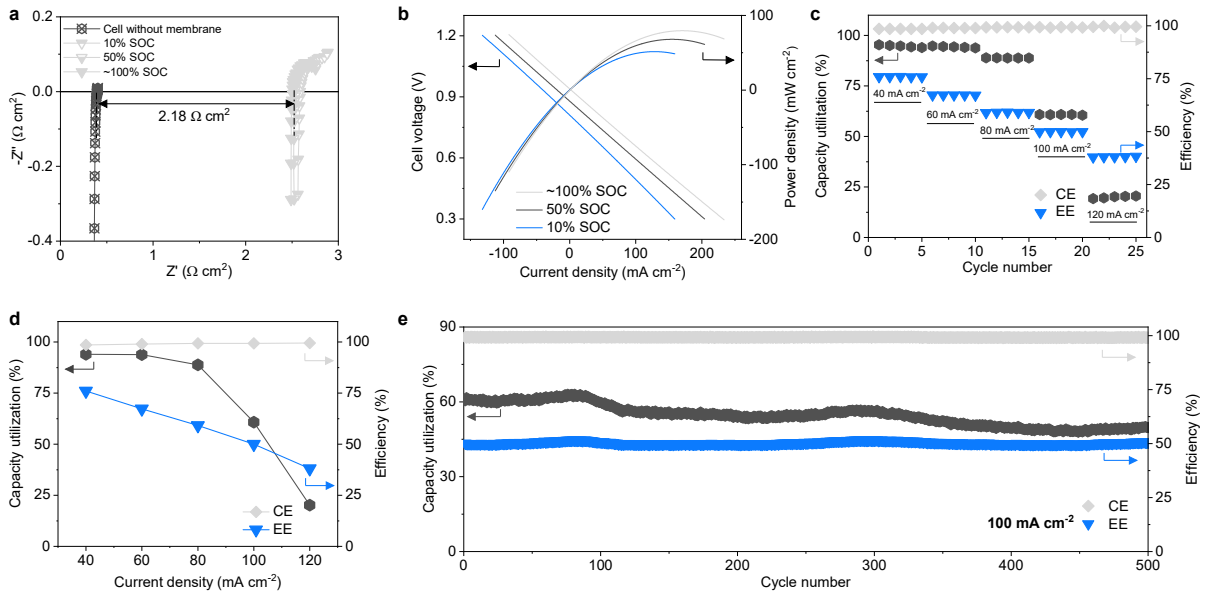

Fig. S32. Performance of a 0.5 M BTMAP-Vi/FcNCl cell assembled with Selemion® AMV membrane. (**a**) EIS spectra and (**b**) polarization curves at various SOCs. (**c, d**) The capacity utilization, Coulombic efficiency (CE), and energy efficiency (EE) at various current densities. (**e**) Long-term galvanostatic cycling of the cell over 500 cycles (59.4 h) at 100 mA cm^{-2}. The capacity utilization, Coulombic efficiency, and energy efficiency are plotted against the cycle number.

Notes: At 0.5 M, the BTMAP-Vi/FcNCl cell assembled with the Selemion® AMV membrane showed a high capacity fade rate of 0.036% per cycle (0.30% per h) over 500 cycles (59.4 h) at 100 mA cm^{-2}.

Table S1. The hydration number (λ), water uptake (WU), Cl^- conductivity (σ_{Cl^-}) at 30 °C and activation energy (E_a) of QCTFs membranes, compared with framework membranes, PIM-based membranes and flexible polymer membranes at 30 °C, 25 °C or room temperature.

Membrane	hydration number (λ)	Water uptake (WU, %)	σ_{Cl^-} (mS cm^{-1})	Activation energy (E_a, kJ mol^{-1})	Reference
M-QCTF	2.1±0.1	8.5±0.3	26±0.5	13±0.7	this work
P-QCTF	1.8±0.1	7.7±0.3	20.3±0.5	15±0.5	
QCTF	3.5±0.1	6.9±0.3	13.2±0.6	20.6±0.6	
Sustainion® X37-50	37.9±3.9	172±18	30.5±0.4	14.5±0.7	
Selemion® DSV	8.1±0.1	29.1±0.4	14±0.5	22.2±0.7	
Selemion® AMV	5.5±0.2	18.7±0.5	7±0.5	24±0.4	
COF-QA-2	19.7	79.49	43.4±3.1	19.2	1
COF-QA-4	19.3	73.4	36±4	19.5	
COF-QA-6	16.9	63.93	28.1±3.6	20.2	
COF-QA-EO	20.1	74.44	38.6±2.7	19.9	
Q-TPF-TBP	4.4	16.6	22.6	17.4	2
MTCP-30	8.5	38.7	23	23.7	3
MTCP-50	9.2	41.9	29	21.2	
MTCP-70	8.9	40.5	18.7	23.1	
DMBP-QTB	not given	not given	16.9	30.6	4
DMDPM-QTB	not given	not given	29.4	17.9	
Trip-QTB	not given	not given	19.6	14.5	
PIM-TDQTB-20	not given	not given	7.4	18.1	5
PIM-TDQTB-50	not given	not given	13	17.9	
PIM-TDQTB-80	not given	not given	25.8	17.3	
PIM-TDQTB-100	not given	not given	27.1	16.9	
PBI_1-$PVBC_1$-NMPD/Cl	11.4	31	10.5	24.7	6
PBI_2-$PVBC_1$-NMPD/Cl	3.3	13.2	5.3	22.4	
SEBS-TMA	2.72±0.18[a]	12.5±4.14[a]	4.6±0.31[a]	not given	7
SEBS-N2C6	3.3±0.25[a]	17.2±5.61[a]	5.7±0.44[a]	not given	
SEBS-N2C3	4.71±0.21[a]	28.6±8.3[a]	8.9±0.4[a]	not given	
SEBS-N2C4	3.53±0.25[a]	22.4±6[a]	6.6±0.47[a]	not given	
SEBS-P2C6	3.26±0.15[a]	20.1±8.43[a]	6.45±0.3[a]	not given	
SEBS-P2O6	6.19±0.29[a]	36.8±7.35[a]	11.7±0.54[a]	not given	
Tokuyama A201	3.92[a]	19[a]	12[a]	not given	
MPRD	65±7[b]	159±17[b]	5.17	37.6	8
MPRD-DT7.5	24±3[b]	49±3[b]	not given	23.8	
MPRD-DT12.5	not given	not given	not given	32.7	
TTMPP	not given	not given	not given	72.4	
MPY	not given	not given	4.35	37.7	
PS	16.7±1.3	25.5±2	7.91	25.91	9
Small	5[b]	4.7±1.7[b]	2.1	23.7	10
Medium	11[b]	17.4±6.2[b]	not given	24.7	
Large	46[b]	100±12.7[b]	52.8	21.1	
HQPSf-CDIC-0	12.5[b]	34.29±1.01[b]	12.90±0.46[b]	not given	11
HQPSf-CDIC-1	14.13[b]	38.04±0.70[b]	14.90±0.10[b]	not given	
HQPSf-CDIC-2	14.83[b]	39.05±0.48[b]	17.00±0.27[b]	not given	
HQPSf-CDIC-3	16.16[b]	42.33±1.48[b]	14.70±0.17[b]	not given	
HQPSf-TMHDA-1	10.3[b]	27.86±0.77[b]	9.19±0.28[b]	not given	
HQPSf-TMHDA-2	8.05[b]	21.75±0.76[b]	8.73±0.43[b]	not given	
RC-QPPO	12.9	37.4	11.2	18.3	12
VPPO/VBC(2.0)-IPN	1.4[a]	3.2[a]	13	14.7	13
$PVBC_{49}$-r-$PBeS_{50}$	16.8	80	16.9[a]	not given	14
$PVBC_{44}$-b-$PBeS_{44}$	14.4	70	18.4[a]	not given	
$PVBC_{100}$-b-$PBeS_{107}$	12.7	60	17.6[a]	not given	

$PVBC_{100}$-b-$PBeS_{183}$	12.5	45	11.6[a]	not given	
X60Y15C6	7.7±0.5[b]	31±2[b]	8.9±0.4[b]	not given	
X60Y30C6	5.9±0.5[b]	22±2[b]	6.7±0.5[b]	not given	
X60Y30C10	5.2±0.5[b]	21±2[b]	5.4±0.3[b]	not given	
X60Y30C16	4.8±0.5[b]	18±2[b]	4.9±0.2[b]	not given	
X80Y20C6	8.1±0.8[b]	43±4[b]	14.9±1.2[b]	not given	15
X80Y40C6	9.1±0.6[b]	30±3[b]	10.9±0.5[b]	not given	
X80Y40C10	4.4±0.2[b]	20±1[b]	7.6±0.4[b]	not given	
X80Y40C16	2.8±0.2[b]	12±1[b]	4.8±0.3[b]	not given	
X60Y60	4±0.8[b]	15±3[b]	4.2±0.2[b]	not given	
X80Y80	3.3±0.5[b]	13±2[b]	5.8±0.3[b]	not given	
m-XPTPA10-2N	15.6±0.6	79±3	20.5±0.3	17.9	
m-XPTPA20-2N	14.7±0.8	71±4	17.5±1.1	20.3	
m-XPTPA30-2N	12.3±1.1	58±5	15.7±0.1	21.9	16
m-XPTPA40-2N	10±0.4	45±2	14.9±0.1	22.7	
m-PTPA-2N	16.4±1.9	88±10	20.6±0.4	15.5	
$^{0.36}Ru_{PEO}$	105±33[b]	169±53[b]	4.1	15.6	
$^{0.55}Ru_{PEO}$	75.4±12.4[b]	152±25[b]	5	16.2	
$^{0.36}Ni_{PEO}$	91±15[b]	162±27[b]	4.3	16.3	17
$^{0.55}Ni_{PEO}$	85±20[b]	193±46[b]	6.1	16.5	
$^{0.36}Co_{PEO}$	86±6.7[b]	154±12[b]	5.2	15.1	
Fumion™	not given	not given	10.1	18	
PFTP-13	not given	not given	23	14.9	
PFTP-0	2.4	not given	28.5	16.6	18
PFBP-0	15.8	not given	28.1	13.9	
PFBP-14	13.3	not given	27.1	14.5	
PQVB-b-PVBF	15.3	46.6	9.5	21.9	19
LDPE-AEM (100 kGy)	20±2	104±9	29.9	16.2	
LDPE-AEM (50 kGy)	20±1	97±5	26.6	15.7	20
ETFE-AEM (30 kGy)	18±2	67±7	24.9	16.3	
PQDP-1	7.5	24	12	15.5	
PQDP-2	7.9	31	15.7	16.1	21
PQDP-3	12.3	54	24	16.8	
PB-g-3PipVBC	not given	not given	8	21.1	
PB-1sphere	not given	not given	20	18.6	22
PB-3sphere	not given	not given	18	19	
PB-5sphere	not given	not given	20	14.1	
PBPA50-3QA	11.9	65.9	23.3	18.2	
PBPA75-2QA	15.3	85.3	18.0	18.6	
PBPA35-3QA	8.4	38.2	15.3	21.3	23
PBPA50-2QA	9.6	42.5	11.5	21.4	
PBPA100-1QA	13.6	61.4	11.2	22	
PFB^+	11[b]	71[b]	26.6	17.9	
PFF^+	5.7[b]	25[b]	12.9	15.9	24
$PFBFF^+$	7.6[b]	40[b]	16.9	21.6	
PPO-22-QA	6.2[b]	17.4[b]	3.3	19.8	
PPO-22-3QA8F	3.4[b]	8[b]	7.6	23.9	25
PPO-8-3QA	2.8[b]	10.2[b]	6.7	14.4	
PBPA-4-QA	8.72	31.7	10.03	23.01	
PBPA-5-QA	8.55	31.4	11.87	22.52	26
PBPA-6-QA	8.2	30.4	12.38	21.94	
PECryp7-Ba	22.2[a]	56[a]	8.4[a]	not given	
PECryp13-Ba	25.2[a]	68[a]	8.8[a]	not given	
PENBCryp11-Ba	6.11[a]	11[a]	4.2[a]	not given	27
PENBCryp14-Ba	8.59[a]	17[a]	4.2[a]	not given	
PENBCryp20-Ba	8.52[a]	23[a]	5.8[a]	not given	
$BrPPO\text{-}DMH^+Cl^-$	1.87±0.88[a]	6.4±3[a]	4.62	not given	28

(Batch #1) BrPPO-DMH^+Cl^- (Batch #2)	4.33±1.85[a]	11.7±5[a]	3.76	not given	
PSF-DMH^+Cl^-	4.44±1.04[a]	12.8±3[a]	20.87	not given	
CMPPO-TMA^+Cl^-	14.67±2.22[a]	26.4±4[a]	5.85	not given	
CMPPO-DMH^+Cl^-	13.83±1.85[a]	22.4±3[a]	4.71	not given	
PSF–TMA^+Cl^--1.98	not given	not given	12.73	30	
PSF–TMA^+Cl^--1.91	not given	not given	10.22	34.88	29
PSF–DMP^+Cl^--1.75	not given	not given	8.92	32.43	
ETFE-g-PVBTMA	3.7±0.2	12.4±0.6	2.4±0.3	24	30
PVB-TMA	not given	not given	5.4±1.8	23.5	
PVB-MPRD	not given	not given	10±1.2	22.1	31
PVB-MPY	not given	not given	12±0.87	21.3	
PAImMM(10)	9.36±0.25	48.2±1.3	16.86	26.9	
PAImMB(11)	6.54±0.44	30.0±2.0	10.13	26	
PAImEE(12)	5.89±0.34	28.1±1.6	12.9	23	32
PAImPP(13)	5.04±0.29	22.3±1.3	6.32	26.9	
PAImBB(14)	2.95±0.48	12.2±2.0	2.74	25.8	
30PPOFC6N	8.45±0.3[b]	28±1[b]	10±1[b]	not given	
40PPOFC6N	11.92±0.81[b]	44±3[b]	12±1[b]	not given	
50PPOFC6N	15.17±1.03[b]	59±4[b]	13±2[b]	not given	
60PPOFC6N	17.94±1.23[b]	73±5[b]	14±2[b]	not given	33
30PPOFC6NC6	8.68±0.69[b]	25±2[b]	12±1[b]	not given	
40PPOFC6NC6	12.55±0.94[b]	40±3[b]	13±2[b]	not given	
50PPOFC6NC6	15±0.88[b]	51±3[b]	15±2[b]	not given	
60PPOFC6NC6	19±1.15[b]	66±4[b]	16±1[b]	not given	
3BQA-1	2.46	5.26	4.56	22.86	
3BQA-2	3.03	7.31	7.7	17.89	34
3BQA-3	3.96	11.34	8.39	20.22	
3BQA-4	11.4	40	15.98	19.82	
HyAEM-MP-180	33	94.2	not given	14.3	35

[a] Measurements at 25 °C. [b] Measurements at room temperature. Other values of hydration number (λ), water uptake (WU) and Cl^- conductivity (σ_{Cl^-}) were obtained at 30 °C.

Table S2. Comparison of energy efficiency (EE, %) and capacity utilization (CU, %) at various current densities between pH-neutral and alkaline AORFBs. The redox chemistry, charge carrier ion and membrane for cell assembly are listed.

Membrane	100 mA cm^{-2}		200 mA cm^{-2}		300 mA cm^{-2}		400 mA cm^{-2}		500 mA cm^{-2}		Transport ion	Concentration	Anolyte/catholyte	Reference
	EE	CU	EE	CU	EE	CU	EE	CU	EE	CU				
M-QCTF	85.3	98.05	76.94	94.33	69.08	89.91	59.10	79.78	49.65	58.78	Cl^-	0.5 M/0.5 M	BTMAP-Vi/FcNCl	this work
Sustainion® X37-50	not given	not given	66.35	76.54	55.3	68.3	42.9	42.7	-	-	Cl^-	0.5 M/0.5 M	BTMAP-Vi/FcNCl	this work
P-QCTF	70.57	87.86	62.04	79.5	49.88	62.19	38.04	28.16	-	-	Cl^-	0.5 M/0.5 M	BTMAP-Vi/FcNCl	this work
SCTF-BP	89	not given	77.3	98	67.7	92.8	58.9	82.5	50.4	62	K^+	0.4 M/0.4 M	DHAQ/$K_4Fe(CN)_6$	[36]
QCTF-BP	77.8	82	66.1	76.1	57.5	62.8	46.2	43.4	-	-	Cl^-	0.5 M/1.0 M	BTMAP-Vi/TEMPTMA	[36]
QPSPBPip-30%	84.3	95	75.2	90.7	63.8	78.5	50.1	45.8	-	-	Cl^-	0.5 M/0.5 M	MV/TEMPTMA	[37]
Selemion® DSV	78.5	96.4	61.17	92.5	48.82	84.4	-	-	-	-	Cl-	1 M/2 M	Dex-Vi/N+TEMPOD	[38]
HC-QPPO	78.3	81	63.9	75.6	50.9	58.14	-	-	-	-	Cl-	0.5 M/1.0 M	BTMAP-Vi/TEMPTMA	[39]
MTCP-50	78	95	60.06	63.74	-	-	-	-	-	-	Cl-	0.5 M/0.5 M	MV/TEMPTMA	[3]
Selemion® DSV	70.89	95.68	47.6	57.06	-	-	-	-	-	-	Cl-	0.5 M/0.5 M	BTMAP-Vi/FcNCl	this work
	43.83	71.24	-	-	-	-	-	-	-	-	Cl-	1.3 M/1.3 M	BTMAP-Vi/BTMAP-Fc	[40]
	55.26	not given	-	-	-	-	-	-	-	-	Cl-	2 M/1.5 M	BHOP-Vi/FcNCl	[41]
	69.36	67.02	-	-	-	-	-	-	-	-	Cl-	0.5 M/0.5 M	BTMAE-Vi/FcNCl	[42]
Selemion® AMV	50	60.74	-	-	-	-	-	-	-	-	Cl-	0.5 M/0.5 M	BTMAP-Vi/FcNCl	this work
	42.05	76.57	-	-	-	-	-	-	-	-	Cl-	0.5 M/0.5 M	MV/FcNCl	[43]
	40	not given	-	-	-	-	-	-	-	-	Cl-	0.5 M/0.5 M	BTMAP-Vi/N2-TEMPO	[44]
	63	87	-	-	-	-	-	-	-	-	Cl-	0.5 M/0.5 M	BTMAP-Vi/TMAP-TEMPO	[45]
	43.2	45.5	-	-	-	-	-	-	-	-	Cl-	0.5 M/0.5 M	MV/4-OH-TEMPO	[46]

"-": cell can't run due to voltage cutoff at the current density.

Table S3. Performance comparison between BTMAP-Vi/FcNCl cells assembled with M-QCTF, P-QCTF, Sustainion® X37-50, Selemion® DSV, and Selemion® AMV membranes.

Membrane	R_{cell} (Ω cm^2)	R_m (Ω cm^2)	Membrane resistance contribution (%)	Electrolyte concentration	Anolyte/catholyte
M-QCTF	0.904	0.23	25.4	0.5 M/0.5 M	BTMAP-Vi/FcNCl
P-QCTF	1.013	0.35	34.6		
Sustainion® X37-50	0.965	0.3	31.1		
Selemion® DSV	1.412	0.74	52.4		
Selemion® AMV	2.799	2.18	77.88		

Notes: R_{cell} referred to area-specific resistance (ASR) of the whole cell derived from the polarization curves at 0 mA cm^{-2}. The membrane resistance (R_m) was obtained by subtracting the resistance (R_{other}) contributed by the electrode, the electrolytes, and the contact resistance from the high-frequency ASR (R_t). R_{other} was measured from cells without a membrane. The membrane resistance contribution was calculated according to $R_m/R_{cell} \times 100\%$.

Table S4. The membrane swelling ratio (SR) at various temperatures.

Membrane	Swelling ratio (SR, %)					
	30 ºC	40 ºC	50 ºC	60 ºC	70 ºC	80 ºC
M-QCTF	1±0.3	1.2±0.3	1.5±0.5	1.8±0.5	2±0.5	2.1±0.7
P-QCTF	0.7±0.3	0.8±0.4	0.9±0.3	1.2±0.3	1.4±0.3	1.7±0.3
QCTF	0.3±0.2	0.4±0.1	0.5±0.3	0.6±0.2	0.8±0.3	0.9±0.3
Selemion® DSV	7.8±0.3	8.3±0.3	8.9±0.3	10±0.4	11±0.3	13.2±0.4
Selemion® AMV	5.3±0.3	5.6±0.2	6.1±0.2	6.4±0.2	6.7±0.2	6.9±0.2
Sustainion® X37-50	54.6±2.9	67.5±2.5	108.3±4.2	-	-	-

Note: The Sustainion® X37-50 membrane broke into pieces because of excessive water uptake at temperatures above 60 ºC.

Table S5. Membrane thickness and the permeability coefficient of redox-active organic electrolyte across different membranes.

Membranes	Membrane thickness (μm)	Permeability coefficient ($cm^2\ s^{-1}$)		Reference
		BTMAP-Vi	FcNCl	
M-QCTF	~ 20	$2.93\pm0.19\times10^{-11}$	$1.44\pm0.04\times10^{-9}$	This work
P-QCTF	~ 20	$3.32\pm0.11\times10^{-11}$	$1.59\pm0.14\times10^{-9}$	This work
QCTF	~ 20	$4.3\pm0.2\times10^{-11}$	$2.04\pm0.08\times10^{-9}$	This work
Sustainion® X37-50	80±5	$2.53\pm0.16\times10^{-7}$	$2.84\pm0.46\times10^{-7}$	This work
Selemion® DSV	~ 95	6.7×10^{-10}	not given	[45]
Selemion® AMV	~ 100	5.4×10^{-11}	not given	[45]
PIM-TDQTB-100	80±5	1.82×10^{-10}	1.946×10^{-9}	[5]
PIM-TDQTB-80	80±5	1.33×10^{-10}	1.693×10^{-9}	
PIM-TDQTB-50	80±5	7.3×10^{-11}	6.03×10^{-10}	
PIM-TDQTB-20	80±5	7.2×10^{-11}	not given	
DMBP-QTB	not given	6.85×10^{-9}	not given	[2]
Q-TBF-TPB	~ 24	4.38×10^{-11}	not given	
QPPO	55	1.46×10^{-10}	not given	[39]
HC-QPPO	133	3.4×10^{-11}	not given	
Fumasep® FAA-3-PE-30	not given	1.82×10^{-10}	not given	[36]

Table S6. Cl^- conductivity, chloride salt permeability coefficient and selectivity for membrane implemented in aqueous organic redox flow batteries.

Membranes	σ_{Cl^-} (mS cm^{-1}) at 30 °C	P_i (cm^2 s^{-1})	Selectivity	Reference
M-QCTF	26±0.5	3.1±0.3×10^{-7}	1.06±0.1×10^4	This work
P-QCTF	20.3±0.5	2.6±0.2×10^{-7}	7.83±0.6×10^3	This work
QCTF	13.2±0.6	1.82±0.3×10^{-7}	4.23±0.7×10^3	This work
Sustainion® X37-50	30.5±0.4	7.4±0.3×10^{-7}	2.9±0.6	This work
Selemion® AMV	7±0.6	1.06×10^{-8}	1.66×10^1 1.96×10^2	[5] The value for P_i is from[5], and selectivity is from[45]
Selemion® DSV	14±0.5	8.37×10^{-8}	1.25×10^2 1.71×10^1 3.22×10^0 5.58×10^1 3.49×10^1	The value for P_i is from[5], and selectivity is from[45] The value for P_i is from[5], and selectivity is from[47]
PIM-TDQTB-100	27.1	3.0×10^{-7}	1.41×10^2 1.65×10^3	[5]
PIM-TDQTB-80	25.2	2.86×10^{-7}	1.45×10^2 2.05×10^3	
PIM-TDQTB-50	12.8	7.4×10^{-8}	7.91×10^2 1.02×10^3	
PIM-TDQTB-20	7.3	1.22×10^{-8}	2.09×10^2 2.14×10^2	
Q-TBF-TPB	22.7	2.14×10^{-8}	4.89×10^2	[2]
QPPO	not given	1.51×10^{-8}	1.03×10^2	[39]
HC-QPPO	not given	4.37×10^{-8}	1.29×10^3	

Notes: Selectivity refers to the ratio of the cross-membrane permeability coefficient between the salt ions (KCl or NaCl) and the bipyridine-based redox-active organic electrolyte.

Table S7. Membrane water uptake (*WU*) at various temperatures.

Membrane	Water uptake (*WU*, %)					
	30 ºC	40 ºC	50 ºC	60 ºC	70 ºC	80 ºC
M-QCTF	8.5±0.3	9.1±0.2	9.6±0.2	10.2±0.2	11.1±0.2	11.4±0.3
P-QCTF	7.7±0.3	8.4±0.3	8.8±0.2	9.2±0.3	9.4±0.2	10.1±0.3
QCTF	6.9±0.3	7.3±0.2	7.5±0.2	7.9±0.2	8.7±0.2	8.9±0.2
Selemion® DSV	29.1±0.4	30.1±0.3	31.3±0.3	32.7±0.4	34.9±0.9	39.3±0.5
Selemion® AMV	18.7±0.5	20.8±0.7	23.2±0.5	24.6±0.5	25.7±0.2	26.5±0.3
Sustainion® X37-50	171.9±17.5	205±11.9	343.5±4	-	-	-

Notes: The Sustainion® X37-50 membrane broke into pieces after 60 ºC.

Table S8. Cl^- conductivity and hydration number for different membranes at various temperatures.

Temperature (ºC)	M-QCTF		P-QCTF		QCTF	
	λ	σ (mS/cm)	λ	σ (mS/cm)	λ	σ (mS/cm)
30	2.14±0.07	26±0.5	1.84±0.06	20.3±0.5	3.46±0.13	13.2±0.6
40	2.29±0.04	30.2±0.4	1.98±0.06	27.4±0.7	3.68±0.09	18.5±0.5
50	2.41±0.04	38.1±0.9	2.09±0.05	32.8±0.5	3.77±0.09	21.7±0.6
60	2.56±0.05	42.2±0.8	2.17±0.06	39.6±0.8	3.96±0.09	27.6±1.3
70	2.78±0.04	49.0±1.0	2.24±0.05	42.3±0.5	4.34±0.09	35.9±0.7
80	2.87±0.07	52.7±1.3	2.39±0.08	48.6±1.1	4.43±0.09	42.8±1.4
Temperature (ºC)	Sustainion® X37-50		Selemion® DSV		Selemion® AMV	
	λ	σ (mS/cm)	λ	σ (mS/cm)	λ	σ (mS/cm)
30	37.9±3.9	30.5±0.4	8.07±0.12	14.0±0.5	5.47±0.15	7.0±0.5
40	45.2±2.6	35.8±0.9	8.35±0.08	17.9±0.3	6.09±0.2	9.8±0.4
50	75.7±0.9	43.6±0.8	8.7±0.08	22.8±0.9	6.78±0.16	12.6±0.4
60	-	-	9.08±0.12	29.4±0.9	7.2±0.14	16.6±0.8
70	-	-	9.7±0.25	37.3±0.8	7.51±0.05	21.2±0.8
80	-	-	10.92±0.15	48.9±2.2	7.75±0.09	27.3±0.8

Note: At temperatures above 60 ºC, the Sustainion® X37-50 membrane broke into pieces because of excessive water uptake.

Table S9. Charge distributions of the QCTF, P-QCTF, and M-QCTF fragments from the restrained electrostatic potential (RESP).

	QCTF		P-QCTF		M-QCTF	
Atomic number	Atom	Charge	Atom	Charge	Atom	Charge
1	C	-0.12413	C	-0.11527	C	-0.11303
2	C	-0.14014	C	-0.13704	C	-0.14198
3	C	-0.15218	C	-0.14333	C	-0.14222
4	C	0.116018	C	0.102538	C	0.11559
5	C	-0.1995	C	-0.19911	C	-0.20369
6	C	-0.11405	C	-0.1053	C	-0.10851
7	C	-0.00334	C	0.030684	C	0.002456
8	C	-0.1175	C	-0.11614	C	-0.0804
9	C	-0.12654	C	-0.06044	C	-0.12051
10	C	-0.16566	C	-0.25098	C	-0.12215
11	C	0.066279	C	0.086811	C	0.075747
12	C	-0.18241	C	-0.16632	C	-0.17538
13	H	0.138554	H	0.138817	H	0.140253
14	H	0.131282	H	0.133427	H	0.132634
15	H	0.151784	H	0.158381	H	0.160021
16	H	0.131077	H	0.1299	H	0.131317
17	H	0.123236	H	0.125482	H	0.117847
18	H	0.144651	H	0.128074	H	0.125143
19	H	0.131591	H	0.129961	H	0.134964
20	N	-0.73481	N	-0.63071	N	-0.38605
21	C	0.857941	C	0.696411	C	0.364508
22	C	0.748991	C	0.795121	C	0.579496
23	C	0.761485	C	0.656738	C	0.438155
24	C	-0.31894	C	-0.33385	C	-0.26325
25	C	-0.05935	C	-0.04263	C	-0.06599
26	C	-0.19848	C	-0.21678	C	-0.19889
27	C	0.062697	C	0.136795	C	0.083977
28	C	-0.37316	C	-0.38751	C	-0.37385
29	C	0.461317	C	0.478973	C	0.481097
30	C	0.079439	C	0.058559	C	0.079001
31	C	-0.14775	C	-0.13984	C	-0.1473
32	C	-0.1439	C	-0.13912	C	-0.14072
33	C	-0.11268	C	-0.10347	C	-0.10699
34	C	-0.14388	C	-0.13764	C	-0.13637
35	C	-0.14247	C	-0.14157	C	-0.14986
36	C	-0.38346	C	-0.30607	C	-0.14189
37	C	0.016227	C	-0.07924	C	-0.1612
38	C	-0.23257	C	-0.17573	C	-0.1383
39	C	0.045663	C	0.071694	C	0.0365
40	C	-0.27951	C	-0.25483	C	-0.22244
41	C	0.381993	C	0.366093	C	0.322616
42	C	0.11164	C	0.085193	C	0.09343
43	C	-0.1666	C	-0.15036	C	-0.15895
44	C	-0.13732	C	-0.1392	C	-0.13466
45	C	-0.12084	C	-0.10475	C	-0.10583
46	C	-0.139	C	-0.14584	C	-0.14823
47	C	-0.1554	C	-0.13816	C	-0.12862
48	H	0.133205	H	0.148984	H	0.151558
49	H	0.137114	H	0.151577	H	0.148924
50	H	0.18031	H	0.183065	H	0.186779
51	H	0.134329	H	0.136822	H	0.137347
52	H	0.135627	H	0.137275	H	0.137441
53	H	0.136734	H	0.137398	H	0.13712
54	H	0.127559	H	0.134469	H	0.134945
55	H	0.099649	H	0.157169	H	0.173164
56	H	0.143117	H	0.143702	H	0.139265
57	H	0.126532	H	0.130383	H	0.125794

58	H	0.137787	H	0.137168	H	0.141841
59	H	0.136319	H	0.138965	H	0.138543
60	H	0.135994	H	0.14031	H	0.141883
61	H	0.133241	H	0.134788	H	0.129251
62	N	-0.71935	N	-0.50768	N	0.002131
63	N	-0.66708	N	-0.58306	N	-0.46656
64	H	0.129805	H	0.130228	H	0.13105
65	H	0.13038	H	0.130741	H	0.130381
66	H	0.127403	H	0.129025	C	-0.33341
67	O	-0.27465	O	-0.24986	H	0.162346
68	C	0.057394	C	0.05167	H	0.162346
69	C	-0.07234	C	-0.06011	H	0.162346
70	C	-0.2124	C	-0.23657	H	0.128235
71	H	0.084998	H	0.093483	O	-0.29927
72	H	0.084998	H	0.093483	C	0.200858
73	H	0.081328	H	0.081987	C	-0.119
74	H	0.081328	H	0.081987	C	-0.17028
75	H	0.152601	H	0.155435	H	0.057973
76	H	0.152601	H	0.155435	H	0.057973
77	N	0.167509	N	0.196224	H	0.082476
78	C	-0.41109	C	-0.44762	H	0.082476
79	C	-0.42084	C	-0.41333	H	0.120686
80	C	-0.2353	C	-0.23925	H	0.120686
81	H	0.192162	H	0.199681	N	0.285149
82	H	0.192162	H	0.199681	C	-0.57591
83	H	0.192162	H	0.199681	C	-0.41892
84	H	0.19041	H	0.191464	C	-0.2865
85	H	0.19041	H	0.191464	H	0.230479
86	H	0.19041	H	0.191464	H	0.230479
87	H	0.160444	H	0.161483	H	0.230479
88	H	0.160444	H	0.161483	H	0.189674
89	H	0.160444	H	0.161483	H	0.189674
90	H	0.049706	H	0.044465	H	0.189674
91	O	-0.36279	O	-0.29265	H	0.168209
92	C	0.021534	C	-0.08171	H	0.168209
93	C	0.134008	C	0.145818	H	0.168209
94	C	-0.28524	C	-0.27508	H	0.028531
95	H	0.091607	H	0.123084	O	-0.34764
96	H	0.091607	H	0.123084	C	-0.01015
97	H	0.0165	H	0.023731	C	0.080524
98	H	0.0165	H	0.023731	C	-0.2304
99	H	0.159098	H	0.157317	H	0.108376
100	H	0.159098	H	0.157317	H	0.108376
101	N	0.252713	N	0.308175	H	0.036542
102	C	-0.39932	C	-0.34952	H	0.036542
103	C	-0.47596	C	-0.48553	H	0.145914
104	C	-0.37052	C	-0.45296	H	0.145914
105	H	0.19828	H	0.181017	N	0.227898
106	H	0.19828	H	0.181017	C	-0.39279
107	H	0.19828	H	0.181017	C	-0.46973
108	H	0.212787	H	0.212295	C	-0.3868
109	H	0.212787	H	0.212295	H	0.197914
110	H	0.212787	H	0.212295	H	0.197914
111	H	0.186027	H	0.20291	H	0.197914
112	H	0.186027	H	0.20291	H	0.212628
113	H	0.186027	H	0.20291	H	0.212628
114			H	0.361456	H	0.212628
115					H	0.194524
116					H	0.194524
117					H	0.194524

Table S10. Energy efficiency (EE, %) and capacity utilization (CU, %) of pH-neutral AORFBs assembled with different membranes and operated at various current densities and various electrolyte concentrations.

Membranes	Anolyte/catholyte	0.1 M anolyte			0.5 M anolyte			Reference
		CD	EE	CU	CD	EE	CU	
M-QCTF	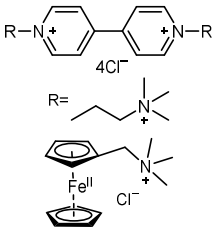	40	91.86	98.70	20	95.81	99.96	This work
		80	85.90	96.11	40	94.08	99.59	
		120	78.49	94.98	60	91.74	99.03	
		160	69.78	87.40	80	89.25	98.48	
		200	61.17	80.10	100	85.30	98.05	
		240	50.30	58.41	200	76.94	94.33	
					300	69.08	89.91	
					400	59.10	79.78	
					500	49.65	58.78	
P-QCTF	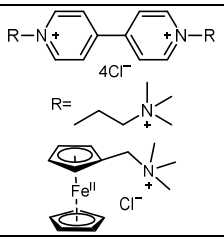	0.1 M anolyte			0.5 M anolyte			This work
		CD	EE	CU	CD	EE	CU	
		40	86.95	96.72	100	70.57	87.86	
		80	77.81	93.91	200	62.04	79.5	
		120	66.64	88.49	300	49.88	62.19	
		160	57.58	80.14	400	38.04	28.16	
		180	53.63	75.13				
		220	42.41	23.73				
QCTF	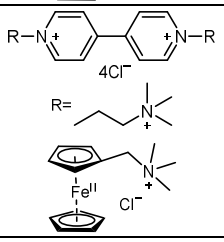	0.1 M anolyte						This work
		CD	EE	CU				
		40	85.43	94.71				
		80	71.61	90.41				
		120	61.53	84.78				
		160	52.86	70.68				
		180	44.94	46.79				
Sustaion® X37-50	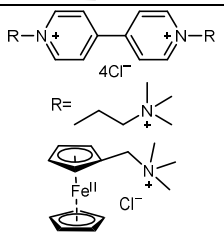	0.5 M anolyte						This work
		CD	EE	CU				
		200	66.35	76.54				
		300	55.3	68.3				
		400	42.9	42.7				
Selemion® DSV	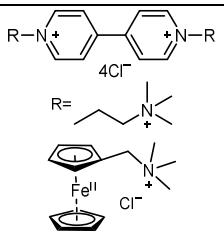	0.5 M anolyte						This work
		CD	EE	CU				
		60	80.29	97.15				
		80	75.5	96.88				
		100	70.89	95.68				
		120	66.2	93.48				
		160	57.25	83.45				
		200	47.6	57.06				
Selemion® AMV	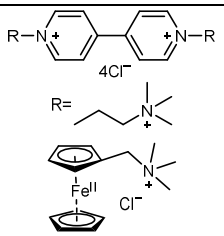	0.5 M anolyte						This work
		CD	EE	CU				
		40	75.97	93.98				
		60	67.3	93.81				
		80	69.13	88.8				
		100	50	60.74				
		120	38.09	20.15				
Selemion® DSV		1.3 M anolyte						[40]
		CD	EE	CU				
		25	81.84	96.3				

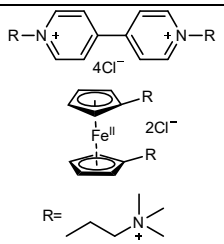	50	66.78	91.97		
	75	54.03	84.97		
	100	43.83	71.24		
	125	36.01	46.54		
	150	29	6.51		

		0.1 M anolyte			2.0 M anolyte		
		CD	EE	CU	CD	EE	CU
Selemion® DSV	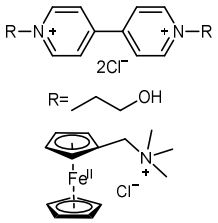	20	89.78	not given	80	63.08	not given
		40	81.16	not given	100	55.26	not given
		60	72.66	not given	120	47.45	not given
		80	64.18	not given	140	29.82	not given
		100	54.32	not given	-	-	-

		0.1 M anolyte		
		CD	EE	CU
Selemion® DSV	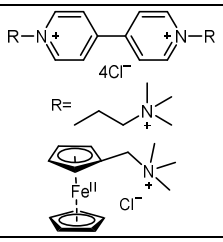	20	90.6	not given
		40	81.7	not given
		60	73.2	not given
		80	64.73	not given
		100	57.31	not given

		0.1 M anolyte		
		CD	EE	CU
Selemion® DSV	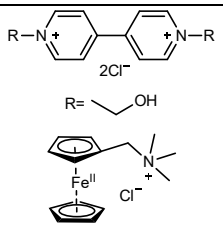	20	92.11	not given
		40	83.76	not given
		60	76.62	not given
		80	68.82	not given
		100	61.97	not given

		0.5 M anolyte			1 M anolyte		
		CD	EE	CU	CD	EE	CU
Selemion® DSV	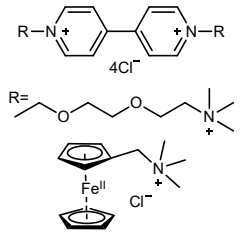	60	80.23	84.93	40	82.94	93.02
		80	74.63	77.76	60	76.61	82.92
		100	69.36	67.02	80	70.73	72.01
		120	62.92	53.21	100	54.19	54.09
		2 M anolyte					
		CD	EE	CU			
		60	73.02	79.48			
		80	67.05	50.01			
		100	60.76	27.6			
		120	50.89	10.1			

		0.1 M anolyte		
		CD	EE	CU
Selemion® DSV	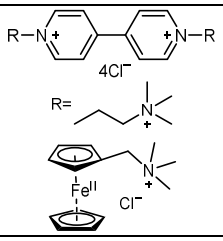	20	89.35	not given
		40	81.84	not given
		60	73.58	not given
		80	65.88	not given

		0.5 M catholyte		
		CD	EE	CU
Selemion® AMV		40	72.06	82.46

	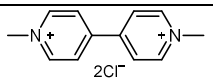 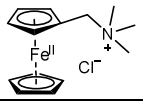	60 80 100	60.11 51.53 42.05	81.34 79.7 76.57	
Selemion® AMV	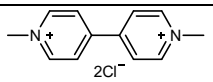 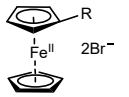 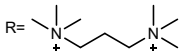	0.5 M catholyte CD 40 60 80 100	EE 70.47 57.57 46.33 36.22	CU 98.66 97.01 92.69 81.64	43
Selemion® AMV	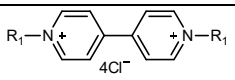 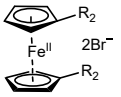 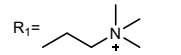 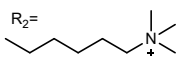	1.5 M catholyte CD 20 30 40	EE 64.04 53.53 42.65	CU 79.02 74.88 70.24	48
Selemion® AMV	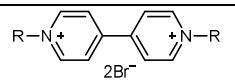 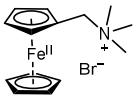 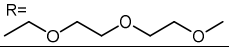	0.5 M anolyte CD 20 30 40 50	EE not given not given not given not given	CU 91.42 86.64 75.67 52.54	49
Selemion® AMV	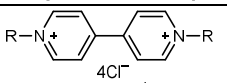 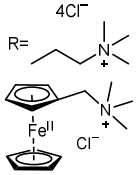	0.1 M anolyte CD 20 40 60	EE 80.03 64.64 46.68	CU not given not given not given	5
AME115	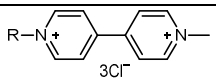 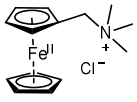 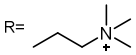	0.25 M anolyte CD 40 60 80 100	EE 76.89 66.15 56.31 46.66	CU 90.22 89.33 86.27 75.82	50
PIM-TDQTB-100	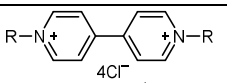 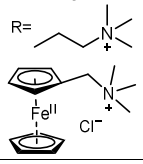	0.1 M anolyte CD 20 40 60 80	EE 91 84.3 76.95 70.08	CU not given not given not given not given	5

		0.1 M anolyte		
		CD	EE	CU
PIM-TDQTB-80	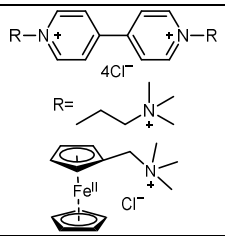	20	88.87	not given
		40	79.9	not given
		60	71.39	not given
		80	63.24	not given
	0.1 M anolyte			
		CD	EE	CU
PIM-TDQTB-50	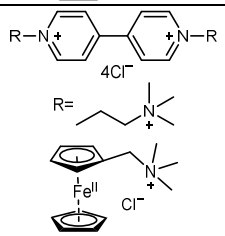	20	86.57	not given
		40	75.3	not given
		60	64.55	not given
		80	54.59	not given
	0.1 M anolyte			
		CD	EE	CU
PIM-TDQTB-20	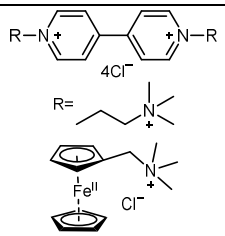	20	75.81	not given
		40	56.71	not given
		60	30.26	not given

Supplementary References

1 He, X. *et al.* De Novo Design of Covalent Organic Framework Membranes toward Ultrafast Anion Transport. *Adv. Mater.* **32** (2020). https://doi.org/10.1002/adma.202001284

2 Liu, J., Wu, W., Zuo, P., Yang, Z. & Xu, T. Ultramicroporous Tröger's Base Framework Membranes for pH-Neutral Aqueous Organic Redox Flow Batteries. *ACS Macro Letters* **13**, 328-334 (2024). https://doi.org/10.1021/acsmacrolett.4c00011

3 Song, W. *et al.* Upscaled production of an ultramicroporous anion-exchange membrane enables long-term operation in electrochemical energy devices. *Nat. Commun.* **14** (2023). https://doi.org/10.1038/s41467-023-38350-7

4 Yang, Z. *et al.* Highly Conductive Anion-Exchange Membranes from Microporous Tröger's Base Polymers. *Angewandte Chemie International Edition* **55**, 11499-11502 (2016). https://doi.org/10.1002/anie.201605916

5 Li, H. *et al.* Ultra-microporous anion conductive membranes for crossover-free pH-neutral aqueous organic flow batteries. *J. Membr. Sci.* **668** (2023). https://doi.org/10.1016/j.memsci.2022.121195

6 Lu, W. *et al.* Piperidinium-Functionalized Poly(Vinylbenzyl Chloride) Cross-linked by Polybenzimidazole as an Anion Exchange Membrane with a Continuous Ionic Transport Pathway. *Ind. Eng. Chem. Res.* **59**, 21077-21087 (2020). https://doi.org/10.1021/acs.iecr.0c04548

7 Xu, Z. *et al.* Novel piperidinium-functionalized crosslinked anion exchange membrane with flexible spacers for water electrolysis. *J. Membr. Sci.* **670** (2023). https://doi.org/10.1016/j.memsci.2022.121302

8 Liu, Y. *et al.* Thin, robust, and chemically stable photo-cross-linked anion exchange membranes based on a polychlorostyrene-b-polycyclooctene-b-polychlorostyrene ABA triblock polymer. *Solid State Ionics* **316**, 135-142 (2018). https://doi.org/10.1016/j.ssi.2017.12.031

9 Amel, A. *et al.* Bicarbonate and chloride anion transport in anion exchange membranes. *J. Membr. Sci.* **514**, 125-134 (2016). https://doi.org/10.1016/j.memsci.2016.04.027

10 Wu, I. *et al.* Enhancing desalination performance by manipulating block ratios in a polyethylene-based triblock copolymer anion exchange membrane for electrodialysis. *J. Membr. Sci.* **647** (2022). https://doi.org/10.1016/j.memsci.2022.120295

11 Jin, Q. *et al.* Cyclodextrin-alkyldiamine rotaxane cross-linked anion exchange membranes for electrodialysis. *J. Membr. Sci.* **706** (2024). https://doi.org/10.1016/j.memsci.2024.122933

12 Hou, J. *et al.* Recyclable cross-linked anion exchange membrane for alkaline fuel cell application. *J. Power Sources* **375**, 404-411 (2018). https://doi.org/10.1016/j.jpowsour.2017.06.073

13 Yang, Z., Hou, J., Wang, X., Wu, L. & Xu, T. Highly Water Resistant Anion Exchange Membrane for Fuel Cells. *Macromol. Rapid Commun.* **36**, 1362-1367 (2015). https://doi.org/10.1002/marc.201500116

14 Wang, L. & Hickner, M. A. Low-temperature crosslinking of anion exchange membranes. *Polymer Chemistry* **5**, 2928-2935 (2014). https://doi.org/10.1039/c3py01490h

15 Zhu, L. *et al.* Crosslinking of comb-shaped polymer anion exchange membranes via thiol–ene click chemistry. *Polymer Chemistry* **7**, 2464-2475 (2016). https://doi.org/10.1039/c5py01911g

16 Jiang, T. *et al.* Dimensionally and oxidatively stable anion exchange membranes based on

bication cross-linked poly(meta-terphenylene alkylene)s. *Polymer* **216** (2021). https://doi.org/10.1016/j.polymer.2021.123433

17 Kwasny, M. T., Zhu, L., Hickner, M. A. & Tew, G. N. Thermodynamics of Counterion Release Is Critical for Anion Exchange Membrane Conductivity. *J. Am. Chem. Soc.* **140**, 7961-7969 (2018). https://doi.org/10.1021/jacs.8b03979

18 Chen, N. *et al.* Poly(fluorenyl aryl piperidinium) membranes and ionomers for anion exchange membrane fuel cells. *Nat. Commun.* **12** (2021). https://doi.org/10.1038/s41467-021-22612-3

19 Hou, J. *et al.* Self-healing anion exchange membrane for pH 7 redox flow batteries. *Chem. Eng. Sci.* **201**, 167-174 (2019). https://doi.org/10.1016/j.ces.2019.02.033

20 Wang, L. *et al.* Non-fluorinated pre-irradiation-grafted (peroxidated) LDPE-based anion-exchange membranes with high performance and stability. *Energy & Environmental Science* **10**, 2154-2167 (2017). https://doi.org/10.1039/c7ee02053h

21 Yang, Y. *et al.* Chemo-stable poly(quinquephenylene-co-diphenylene piperidinium) ionomers for anion exchange membrane fuel cells. *J. Power Sources* **506** (2021). https://doi.org/10.1016/j.jpowsour.2021.230184

22 Zhang, S. *et al.* Enhanced conductivity and stability via comb-shaped polymer anion exchange membrane incorporated with porous polymeric nanospheres. *J. Membr. Sci.* **597** (2020). https://doi.org/10.1016/j.memsci.2019.117750

23 Li, L. *et al.* High Ion Conductivity and Diffusivity in the Anion Exchange Membrane Enabled by Tethering with Multication Strings on the Poly(biphenyl alkylene) Backbone. *ACS Applied Energy Materials* **3**, 6268-6279 (2020). https://doi.org/10.1021/acsaem.0c00409

24 Lee, W.-H., Mohanty, A. D. & Bae, C. Fluorene-Based Hydroxide Ion Conducting Polymers for Chemically Stable Anion Exchange Membrane Fuel Cells. *ACS Macro Letters* **4**, 453-457 (2015). https://doi.org/10.1021/acsmacrolett.5b00145

25 Li, Y. *et al.* Boosting the performance of an anion exchange membrane by the formation of well-connected ion conducting channels. *Polymer Chemistry* **10**, 2822-2831 (2019). https://doi.org/10.1039/c9py00011a

26 Wang, T. *et al.* Towards high alkaline stability and fuel cell performance in anion exchange membranes via backbone−cation alkylene spacer tuning for quaternized poly(biphenylene alkylene)s. *J. Power Sources* **557** (2023). https://doi.org/10.1016/j.jpowsour.2022.232590

27 Zhang, H. *et al.* Alkaline-Stable Anion-Exchange Membranes with Barium [2.2.2]Cryptate Cations: The Importance of High Binding Constants. *Angewandte Chemie International Edition* **62** (2023). https://doi.org/10.1002/anie.202217742

28 Arges, C. G., Wang, L., Jung, M.-s. & Ramani, V. Mechanically Stable Poly(arylene ether) Anion Exchange Membranes Prepared from Commercially Available Polymers for Alkaline Electrochemical Devices. *J. Electrochem. Soc.* **162**, F686-F693 (2015). https://doi.org/10.1149/2.0361507jes

29 Arges, C. G., Parrondo, J., Johnson, G., Nadhan, A. & Ramani, V. Assessing the influence of different cation chemistries on ionic conductivity and alkaline stability of anion exchange membranes. *J. Mater. Chem.* **22** (2012). https://doi.org/10.1039/c2jm14898f

30 Pandey, T. P. *et al.* Interplay between water uptake, ion interactions, and conductivity in an e-beam grafted poly(ethylene-co-tetrafluoroethylene) anion exchange membrane. *Phys. Chem. Chem. Phys.* **17**, 4367-4378 (2015). https://doi.org/10.1039/c4cp05755d

31 Ponce-González, J. *et al.* High performance aliphatic-heterocyclic benzyl-quaternary

ammonium radiation-grafted anion-exchange membranes. *Energy & Environmental Science* **9**, 3724-3735 (2016). https://doi.org/10.1039/c6ee01958g

32 Fan, J. *et al.* Poly(bis-arylimidazoliums) possessing high hydroxide ion exchange capacity and high alkaline stability. *Nat. Commun.* **10** (2019). https://doi.org/10.1038/s41467-019-10292-z

33 Zhu, L., Pan, J., Christensen, C. M., Lin, B. & Hickner, M. A. Functionalization of Poly(2,6-dimethyl-1,4-phenylene oxide)s with Hindered Fluorene Side Chains for Anion Exchange Membranes. *Macromolecules* **49**, 3300-3309 (2016). https://doi.org/10.1021/acs.macromol.6b00578

34 He, Y. *et al.* Achieving high anion conductivity by densely grafting of ionic strings. *J. Membr. Sci.* **559**, 35-41 (2018). https://doi.org/10.1016/j.memsci.2018.05.002

35 Buggy, N. C. *et al.* A Polyethylene-Based Triblock Copolymer Anion Exchange Membrane with High Conductivity and Practical Mechanical Properties. *ACS Applied Polymer Materials* **2**, 1294-1303 (2020). https://doi.org/10.1021/acsapm.9b01182

36 Zuo, P. *et al.* Near-frictionless ion transport within triazine framework membranes. *Nature* **617**, 299-305 (2023). https://doi.org/10.1038/s41586-023-05888-x

37 Zhang, H. *et al.* High-performance spiro-branched polymeric membranes for sustainability applications. *Nature Sustainability* **7**, 910-919 (2024). https://doi.org/10.1038/s41893-024-01364-0

38 Hu, X. *et al.* An operationally broadened alkaline water electrolyser enabled by highly stable poly(oxindole biphenylene) ion-solvating membranes. *Nature Energy* (2024). https://doi.org/10.1038/s41560-023-01447-w

39 Peng, K. *et al.* Constructing Microporous Ion Exchange Membranes via Simple Hypercrosslinking for pH-Neutral Aqueous Organic Redox Flow Batteries. *Angewandte Chemie International Edition* **63** (2024). https://doi.org/10.1002/anie.202407372

40 Beh, E. S. *et al.* A Neutral pH Aqueous Organic–Organometallic Redox Flow Battery with Extremely High Capacity Retention. *ACS Energy Letters* **2**, 639-644 (2017). https://doi.org/10.1021/acsenergylett.7b00019

41 Liu, Y. *et al.* Screening Viologen Derivatives for Neutral Aqueous Organic Redox Flow Batteries. *ChemSusChem* **13**, 2245-2249 (2020). https://doi.org/10.1002/cssc.202000381

42 Kang Peng, P. S., Zhengjin Yang,* and Tongwen Xu*. A PEGylated Viologen for Crossover-Free and High-Capacity pH-Neutral Aqueous Organic Redox Flow Batteries. *Batteries & Supercaps* **6**, e202200426 (2023). https://doi.org/10.1002/batt.202200426

43 Bo Hu, C. D., Zayn Rhodes, and T. Leo Liu*. Long-Cycling Aqueous Organic Redox Flow Battery (AORFB) toward Sustainable and Safe Energy Storage. *J. Am. Chem. Soc.* **139**, 1207−1214 (2017). https://doi.org/10.1021/jacs.6b10984

44 Hu, B., Hu, M., Luo, J. & Liu, T. L. A Stable, Low Permeable TEMPO Catholyte for Aqueous Total Organic Redox Flow Batteries. *Advanced Energy Materials* **12** (2021). https://doi.org/10.1002/aenm.202102577

45 Liu, Y. *et al.* A Long-Lifetime All-Organic Aqueous Flow Battery Utilizing TMAP-TEMPO Radical. *Chem* **5**, 1861-1870 (2019). https://doi.org/10.1016/j.chempr.2019.04.021

46 Liu, T., Wei, X., Nie, Z., Sprenkle, V. & Wang, W. A Total Organic Aqueous Redox Flow Battery Employing a Low Cost and Sustainable Methyl Viologen Anolyte and 4-HO-TEMPO Catholyte. *Advanced Energy Materials* **6** (2015). https://doi.org/10.1002/aenm.201501449

47 Wang, L. *et al.* Highly Soluble TEMPO-Viologen Bipolar Molecule for Ultra-Stable Aqueous Redox Flow Batteries. *Adv. Funct. Mater.* (2023). https://doi.org/10.1002/adfm.202310620

48 Qianru Chen, Y. L., Yahua Liu, Pan Sun, Zhengjin Yang,* Tongwen Xu*. Designer Ferrocene Catholyte for Aqueous Organic Flow Batteries. *ChemSusChem* **14**, 1295–1301 (2021). https://doi.org/10.1002/cssc.202002467

49 Yao, Y. *et al.* Nonionic oligo(ethylene glycol)-substituted viologen negolytes for aqueous organic redox flow batteries. *J. Mater. Chem.A* **11**, 12984-12991 (2023). https://doi.org/10.1039/d2ta09177a

50 DeBruler, C. *et al.* Designer Two-Electron Storage Viologen Anolyte Materials for Neutral Aqueous Organic Redox Flow Batteries. *Chem* **3**, 961-978 (2017). https://doi.org/10.1016/j.chempr.2017.11.001